HIGH ENERGY LASER WINDOWS

Naval Research Laboratory
Washington, D. C.

31 December 1972

High Energy Laser Windows

Semi-Annual Report No. 3
For period ending 31 December 1972

Sponsored by
Advanced Research Projects Agency
ARPA Order [illegible]

NAVAL RESEARCH LABORATORY
Washington, D.C. 20375

ARPA Order
2031

Program Code
3D10

Principal Investigator:
R. W. Rice
(202)767-2131

Contractor:
U. S. Naval Research Laboratory

Effective Date of Contract:
1 July 1972

Contract Expiration Date:
30 June 1973

Amount of Contract:
$200K

The views and conclusions contained in this document are those of the authors and should not be interpreted as necessarily representing the official policies, either expressed or implied, of the Advanced Research Projects Agency or the U. S. Government.

Forward and Acknolwedgments

This semi-annual technical report summarizes work performed by personnel of the U. S. Naval Research Laboratory, Washington, D.C. 20375 , under ARPA Order 2031. The program was coordinated by Mr. R. Rice and Dr. P. Becher and monitored by Dr. C. M. Stickley of ARPA. The report covers the period 1 July 1972 through 31 December 1972.

The following members of the NRL technical staff are acknowledged for their contributions to the program: F. von Batchelder and J. Allard in the crystal preparation, S. Slawson and B. Speronello in the press forging studies, W. Vaughan and W. Cullen in the scanning electron microscopy studies, and O. Imber in the absorption studies.

TABLE OF CONTENTS

1.0.	INTRODUCTION AND SUMMARY	1
2.0.	MATERIALS PREPARATION	3
	2.1. Crystal Growth and Analysis	3
	2.2. Press Forging Studies	10
	2.3. Chemical Polishing	23
3.0.	STRENGTH AND FRACTURE OF SINGLE AND POLYCRYSTALLINE KCl	33
4.0.	OPTICAL ABSORPTION STUDIES AT 10.6μm	48
	4.1. Calorimetry	49
	4.2. Absorption Measurements	59
5.0.	THEORETICAL ANALYSIS	65
	Multiphonon Absorption by Ionic Crystals: Temperature Dependence	

1.0. INTRODUCTION AND SUMMARY

The goal of this program is to improve the strength and fracture behavior of alkali halides while retaining their low absorption for laser window use. The approach of plastically deforming single crystals by press forging to obtain a fine grain polycrystalline body has been previously shown to increase yield stresses by an order of magnitude (to about 5000 psi). In this report, further advances in raising strengths and lowering absorption are presented.

Previous strength results have been confirmed, and the feasibility of further strengthening by alloying and possibly by texturing press forged bodies has been demonstrated. Improved understanding of microstructure formation and grain growth has been obtained and used to develop a more homogeneous microstructure by appropriate reforging. These same press forged KCl bodies have been shown to have about an order of magnitude higher fracture energy (i.e., toughness) than single crystals.

Calorimetric absorption measurement and chemical polishing techniques have been improved. Application of these has corroborated the lower absorption coefficients (e.g. 0.0005-0.0008 cm^{-1}) achieved in purer KCl and shown that very low levels of surface absorption can be obtained by chemical polishing. Measurements on press forgings have shown that much lower absorption coefficients result when purer starting crystals are used. However, measurements at different locations on the forgings have shown quite variable absorption values contrary to the starting crystal results. This variability has prevented clear separation of surface and bulk absorption. A fractional power absorbed ($\beta\ell$) of 0.005 has been measured on a TlCl crystal, but the absorption in purified samples might be lower. An important theoretical development for KCl has shown that intrinsic and extrinsic absorption effects should have different temperature dependences, and hence be separable by absorption-temperature studies.

A major emphasis of continuing work will be to determine the source of variable absorption and to minimize it by surface and bulk studies. Effects on absorption in forged bodies of varying surface finish and improved chemical polishing will be studied. Bulk studies will be directed at detecting and minimizing any internal causes of variable absorption. Such studies will include the effects of post-annealing and forging atmospheres and the

use of analytical techniques such as Auger and IR spectroscopy.

Efforts on purification - especially of alloy crystals - will continue, as will forging, alloying, and texturing studies. The effects of these and of irradiation on strength-fracture behavior and absorption will be examined. Studies of absorption as a function of temperature will be carried out in an attempt to separate intrinsic and extrinsic effects. Further exploratory studies of other materials, including BaF_2 for the 3-5 μm region, will continue.

2.0 MATERIALS PREPARATION

2.1. Crystal Growth and Analysis, P. H. Klein

2.1.1. Introduction

The purpose of this phase of the work is to prepare special materials, primarily crystals, that are otherwise not available. This includes three tasks: Preparation of purer crystals, alloy crystals, and new materials. Because of the availability of purified crystals from other laboratories (e.g., see Sections 2.2, 3.0 and 4.0), purification has not been emphasized in this period. However, work on zone refining KCl is in progress.

2.1.2. Preparation of Strontium-doped KCl

Crystal Growth

KCl crystals containing 0.1, 0.5, 0.75, and 1.0 mole percent $SrCl_2$ were selected, based on work of Chin et al (1) (see Sections 2.2 and 3.0). Harshaw KCl crystals and twice-recrystallized $SrCl_2$ (reagent grade) were used as starting materials. No attempt was made to diminish the hydroxyl content of these materials for growth of initial specimens. Charges of approximately 80 g each were melted in platinum crucibles using an r-f induction heater and an A. D. Little Type MP crystal-growing furnace. Argon, purified by passage over titanium at 800-900°C, was admitted to the furnace at selected pressures ranging from 0.2-1.0 atm. Lower pressures favored visibility of the growth process, but at the expense of increased evaporative loss. Nucleation took place on seeds of undoped KCl. Pulling rates for the Czochralski growth were 1.25-2.5 cm/h with constant rotation in the 4-7 rpm range.

Regardless of the amount of $SrCl_2$ present in the melt, all crystals were transparent during their first 2.0-2.5 cm of growth. As the crystal length increased beyond that point, crystals containing 0.75 mole percent or more $SrCl_2$ developed a cloudiness, while maintaining transparency in the lowest 2.0-2.5 cm. Cloudiness extended the full length of more heavily doped crystals after they had been withdrawn from the melt and allowed to cool. Specimens which reached a length of three or more centimeters without developing a cloudy region remained transparent after cooling.

Figure 1 shows representative specimens of as-grown KCl-$SrCl_2$ single crystals produced in this way. The crystal containing 0.75 mole percent $SrCl_2$ shows clearly the

demarcation between cloudy and clear regions. The diameter of the cloudy region may be seen to vary in this example ("C" in the photograph). Pulling-log entries suggest that changes in diameter of the clouded region correspond to changes in pulling rate or, less frequently, to adjustments of melt temperature.

Cross-section views of clouded crystals are shown in Fig. 2. The sharpness of the separation between clouded and clear regions is noteworthy, as is the regularity of the figure produced by the opacified region. These observations are consistent with the hypothesis that precipitation of dopant, at a temperature intermediate between the melting point and room temperature, is responsible for clouding. With this hypothesis, it is possible to use published information to derive methods for selecting compositions which tend to minimize opacification during the press-forging operation.

Discussion of $KCl-SrCl_2$ Phase Composition

All three published phase-equilibrium studies dealing with the $KCl-SrCl_2$ system (2-4) agree that two compounds are formed and that one of them, K_2SrCl_4, melts between 595° and 600°C. It is likely that the precipitates shown in Figs. 1 and 2 have this composition. A relatively recent study (5) of the kinetics of precipitation in this system reveals that both the solubility of K_2SrCl_4 and the rate at which it precipitates in KCl are each extremely dependent on temperature. This observation makes it possible to explain the appearance of a "core" in crystals C and D of Fig. 1. Cooling of the outer portion of the crystal during growth was so rapid that the diffusion required for precipitation of K_2SrCl_4 could not take place. In the central portion of the boule, however, temperatures remained sufficiently high for precipitation to occur, once the solubility limit had been exceeded.

These observations have extreme importance for press-forging. It may be concluded that it is possible to exceed the equilibrium solubility limit, provided that temperatures are kept below the range in which diffusion (and agglomeration) can take place. This point can be illustrated by a specific example.

The solubility data of Rogalla and Schmalzreid (5) can be expressed in the form

$$\log_{10} M_{Sr} = \frac{-6820}{T} + 6.39 \qquad (1)$$

Here, M_{Sr} is the mole fraction of $SrCl_2$ in the KCl-$SrCl_2$ mixture, and T is in degrees Kelvin. The consequences of Equation (1) are that precipitates should appear at equilibrium if the $SrCl_2$ mole fraction exceeds 0.08 (8 mole percent) at 635°C; 0.0035 (0.35 mole percent) at 500°C; 180 ppmA at about 400°C; and 3 ppmA at 300°C. However, because precipitation is diffusion-controlled, and because the diffusion coefficient is small and exponentially dependent on temperature, precipitation does not readily occur below 400°C. It then becomes possible to consider incorporation of 100-200 ppmA of Ba and Sr in clear KCl crystals (6), despite the fact that room-temperature equilibrium solubility would be grossly exceeded.

Press-forging results obtained during the current reporting period show that incorporation (about 0.1 mole percent) of strontium chloride in potassium chloride crystals greatly increases the strength of polycrystalline forgings (see Section 3.0). Smaller concentrations would make it possible to take advantage of this observation, while diminishing the risk of precipitation and introduction of light-scattering centers.

2.1.3. Thallous Chloride

While the alkali halides have lower absorption than other halides, it is not known whether this is an intrinsic difference, or due to less purification of other halides. Thallium halides would be possible candidate window materials if the absorption could be reduced. They would be attractive because they are not deliquescent. It was therefore decided to investigate absorption in pure thallium halide crystals such as TlCl.

While TlCl is most often used in infrared applications as a constituent of KRS-6, its optical absorption in the 10.6 micrometer region has not, to our knowledge, previously been determined by laser calorimetry. A crystal, grown several years ago at the Naval Research Laboratory by the Bridgman process, was available for study, and was sliced, as shown in Fig. 3, before being made into bars for calorimetric study.

The plate of TlCl shown in Fig. 3 consisted mainly of a slab about 1 cm thick. The photograph shows clearly the nucleating point and the impurities which were carried to the surface during Bridgman growth. One objective of this measurement was to determine whether inaugurating a stringent purification program might not raise the quality of thallous chloride to the point at which it could be

considered for press-forging or for alloying into window materials which would be free of scattering centers. The results, which are discussed further in Section 4.2., are, unfortunately, inconclusive.

Briefly, the fractional power ($\beta\ell$) absorbed was about 0.005 for both a 1-cm and a 2-cm piece. This observation suggests that surface absorption is dominant, and that the bulk absorption may be considerably less. Samples with much less internal scattering and much less surface absorption would be required for reliable determination of bulk absorption.

It should be borne in mind that the absorption on this TlCl crystal is quite comparable to that obtained with ordinary samples of KCl which have been polished by ordinary infrared-cell window polishing techniques. The thallous chloride specimen had more scattering than would be expected with KCl. The scattering centers may have resulted from minor photolysis that occurred during the 21 years since growth of the boule. One can only conclude that further study of fresh, purified crystals is needed to determine to what extent 10.6 micrometer absorption could be reduced.

2.1.4. Future Materials Preparation

Emphasis will be placed on growth of KCl-$SrCl_2$ crystals containing only 50-250 ppmA of strontium because of the promising forged strengths expected from these (see Section 3.0). These will be prepared from KCl which has been treated with chlorine and zone-refined under HCl in order to minimize hydroxyl contamination. Some additional activity on other binary halides, including those containing thallium, is planned, but will be primarily exploratory in nature.

1. G. Y. Chin, L. G. Van Uitert, M. L. Green and G. Zydzik, "Hardness, Yield Strength and Young's Modulus in Halide Crystals," Scripta Met. 6, 475 (1972).
2. E. Vortisch, "Mixed Crystals in the Ternary Systems Formed by Strontium Chloride, Barium Chloride, and Sodium or Potassium Chloride," Neues Jahrb. Min. Geol. 38, 185 (1914).
3. E. P. Dergunov and A. G. Bergman, "Complex Formation between Chlorides of Alkali and Alkaline-Earth Metals," Doklady Akad. Nauk S.S.S.R. 75, 815 (1950).

4. G. A. Bukhalova and V. M. Burlakova, "The K^+ Li^+, Sr^{2+} || Cl^- System," Zh. Neorgan. Khim., 11, 164 (1966); translation in Russ. J. Inorg. Chem. 11, 87 (1966).

5. W. Rogalla and H. Schmalzried, "Precipitation Kinetics of Supersaturated KCl-$SrCl_2$ Crystals," Ber. Bunsenges. Physik. Chem. 72, 615 (1968).

6. K. H. Rosette, C. F. Swinehart, and E. F. Shrader, "Divalent-Ion Doping of Polycrystalline KCl," presented at the Conference on High-Power Infrared Laser Window Materials, Hyannis, Mass., October 31, 1972.

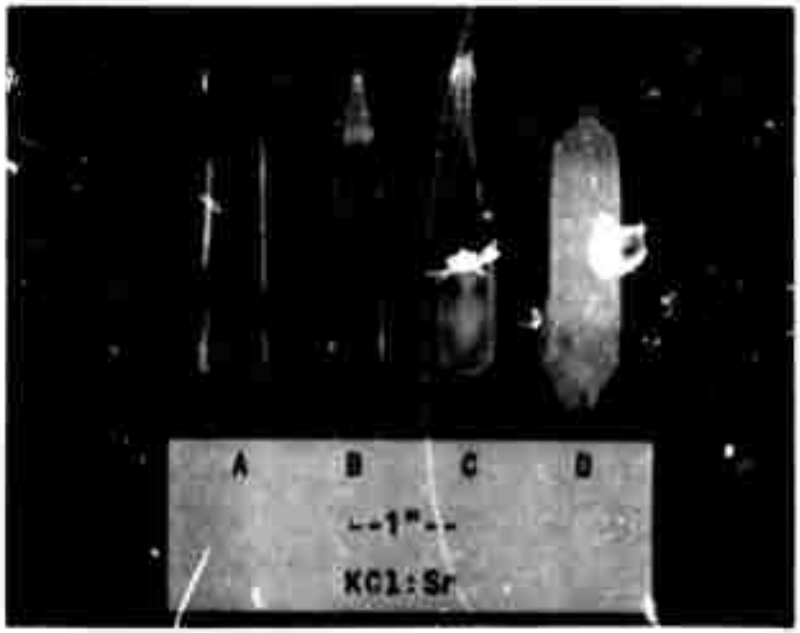

Fig. 1. As-grown single crystal boules of potassium chloride containing the following amounts of strontium chloride (in mole percent): A - 0.2; B - 0.5; C - 0.75; and D - 1.0.

Fig. 2. Cross-sections of the two most heavily doped crystals of Fig. 1, showing regions in which precipitation, presumably of K_2SrCL_4, has taken place. This can take place when cooling through the saturation temperature is sufficiently slow to permit diffusion of strontium and agglomeration of precipitates. Cooling of the outermost parts of the crystals is too rapid for such diffusion to occur.

Fig. 3. Bridgman-grown thallous chloride single crystal, grown at the Naval Research Laboratory in 1950-51. Impurities, swept to the upper surface of the boule during growth, can be seen at the top of the photograph. Slab thickness is about 1 cm.

2.2. Press Forging Studies, P. F. Becher and R. W. Rice

2.2.1. Introduction

The present forging studies emphasized the further strengthening of halides by press forging and development of techniques and basic knowledge required for large scale forgings. Grain size reductions to 5 μm in KCl have resulted in yield strengths of about 5000 psi; however, significant increases in strength by further grain size refinement were felt to be impractical. Additional strengthening has been sought by forging alloyed crystals and by altering the as-forged texture (i.e., the degree and type of grain alignment).

Slow post-forging cooling cycles and thermal gradients and non-homogeneous deformation during forging can adversely affect the resultant microstructure. These effects, such as limiting both grain size refinement and homogeneity, are likely to increase as the size of the forging increases from the present ≈2" diameter by ≈1/4" thick specimens. Thus, a more detailed knowledge of forging and annealing phenomena that control microstructure is necessary for successful press forging scale-up. It is recognized that even with this understanding and control, greater microstructural inhomogeneity can be expected in larger forgings. Thus, reforging studies were initiated to improve microstructural homogeneity.

2.2.2. Experimental Technique

Commercially grown non-laser grade KCl crystals* were used in most of the press forging studies, while a limited number of forgings were made from a high purity KCl boule**. The Sr-doped KCl crystals, growth of which is discussed in Section 2.1, were selected for initial alloy studies. Small BaF_2 crystals* were used in the press forging studies of alkaline earth halides.

* Harshaw Chemical Company.

** R. C. Pastor and colleagues, Hughes Research Laboratory.

Cleaved crystals with 2:1 aspect ratios were water-polished to remove surface flaws, then forged generally along <100> axes in the range of 125° to 200°C, as previously described (1,2). Some <110> and <111> axis forgings were also carried out. Resultant compressive deformation (with unconstrained lateral flow) at constant strain rate ($5x10^{-2}min^{-1}$) yielded disks up to 2" in diameter and 1/4" thick, at pressures of less than 5000 psi. The completed forgings were ejected from the press, rapidly cooled to 100°C to minimize grain growth, annealed at 100°C to relieve strains, then slowly cooled to avoid quenching strains. With this technique, fifty forgings of various materials and sample sizes were completed since the previous report.

This technique repeatedly resulted in crack-free forging (Fig. 1a) with the use of lubricants which relieved end constraint forces during forging. Pyrolytic graphite foil and silicone sprays were found to have good lubricity; however, the silicone sprays were limited to use at temperatures less than 250-300°C and may act as absorbing surface species if not adequately removed from the forging. High end constraint forces and inadequate removal of surface flaws resulted in edge tearing and associated cracks which generally aligned with the <100> direction (Fig. 1b). Forgings of circular cross-section crystals were less likely to tear than square crystals as a result of more uniform peripheral stresses developed during forging. Enhancing plastic flow by increasing the temperature, reducing strain rate, and decreasing strain also was effective in eliminating tearing or cracking. Thus, compressive strains of 70% or greater required forging temperatures approaching 200°C to avoid cracking, while improvements in end face lubricants and crystal shape diminished these requirements. As edge tearing problems could be avoided by several other means, most forgings involved square prism crystals for convenience in reforging experiments discussed later.

2.2.3. Results and Discussion

As microstructure (average grain size, grain size uniformity, grain shape) plays a major role in the properties

of materials, a better understanding of how processing and starting crystal characteristics can affect microstructure was sought. The following subsections are concerned with the effects of (1) forging temperature and strain, (2) reforging, (3) crystal orientation, and (4) alloying on the microstructure developed by press forging.

Temperature and Strain Effects

The forging temperature and amount of forging strain were independently changed to study their influence on the development of a polycrystalline microstructure (primary recrystallization), as well as on exaggerated grain growth (secondary recrystallization). Temperatures of 125°, 150°, and 200°C were used in forging <100> axis KCl crystals to strains of ≦30, 40, 50, 60 and ≧70% at a constant strain rate of $5 \times 10^{-2} min^{-1}$ using pyrolytic graphite lubricant shims.

The results demonstrated that when the temperature is constant (125°, 150°, or 200°C), increasing strains change the microstructure from a deform crystal (25% strain) to a polycrystal (40% strain) (Fig. 2). Thus, recrystallization required strains of 30-40% with larger strains acting to refine the grain size. However, when the forging strains increased above 60%, exaggerated grain growth occurred (Fig. 2D). At constant strains, increasing the forging temperature influenced the microstructure primarily at low strain levels. Thus, increasing forging temperatures for 25-30% strain promoted the formation of a polycrystalline microstructure (Figs. 2a, 3a, and 4a). At higher strain levels (>40%), increasing the forging temperatures had little effect on the microstructure (Fig. 3,4). However, increasing the forging temperature resulted in greater plasticity of the specimen and thus reduced fracture and tearing of the forging.

Previously exaggerated grain growth has been observed in forgings deformed more than 60% (1,2). Bernal and coworkers (3) have also observed this behavior and have shown that the boundaries of large, idiomorphic grains in highly strained (80%) forgings were mobile at room temperature. They also found that the rate of boundary migration passed through a maximum at about 50°C. They attributed the subsequent decrease to recovery, a thermally activated process which relieves strain by rearrangement of dislocations. Previous work in the present study (1,2) showed that post-forging anneals at 100-125°C improved the plasticity of the polycrystalline samples without significantly changing their room temperature yield strength.

Both of these observations indicate that increasing the forging strain above 60% resulted in residual internal strain in the polycrystalline bodies which then could be relieved at about 100°C by recovery processes.

To determine if residual strain was a function of the forging strain and if residual strain was related to exaggerated grain growth, hardness data were obtained on the previous temperature-strain study forgings. Above 40% forging strain, the hardness increased rapidly as a function of forging strain, indicative of increasing residual strain hardening. A maximum in hardness occurred at or just prior to forging strains where exaggerated grain growth occurred (≧60%), then a decrease in hardness occurred which was accompanied by exaggerated grain growth as the forging strain increased. This behavior indicates that the residual strain produced by dislocation interactions reaches a critical level where exaggerated grain growth is initiated as a result of the residual strain energy. The strain energy, and thus residual strain, then is reduced by continued exaggerated grain growth resulting in the hardness decreases. This is indicative of strain-induced exaggerated grain growth. It also points out that exaggerated grain growth can be avoided by eliminating residual strain by either limiting the forging strain, thus keeping residual strain below that for exaggerated growth or annealing to remove residual strains. Thus, annealing to eliminate the residual strain not only reduces exaggerated grain growth, resulting in more uniform grain size and resultant mechanical properties, but reducing residual internal strains also results in more ductile polycrystalline bodies.

Reforging

Initial studies of forging polycrystalline KCl* resulted in the highest yield strength (5500 psi) for polycrystalline KCl (1,2). Subsequent observations suggested that the polycrystalline character of the starting billet resulted in a more uniform microstructure and greater misorientation between grains. Thus a study of reforging was initiated where KCl crystals were initially forged in a <100> direction to either 30, 40, or 50% strain at temperatures of 125°, 150°, or 200°C. These samples were next annealed at 300°C to develop a polycrystalline microstructure and subsequently reforged in an orthogal direction at 200°C to strains of 65-70%.

*Fusion-cast KCl furnished by R. C. Pastor and colleagues, Hughes Research Laboratory.

These reforged bodies (Fig. 5) exhibited two subtle differences: (1) a more equiaxed grain structure, and (2) a more uniform grain size distribution as compared to the previous single axis forgings, while reforging along the original forging axis resulted in extensive exaggerated grain growth.

The more uniform microstructure of reforged KCl was seen to result as follows: (1) the anneal resulted in a stabilized, recrystallized microstructure which deformed readily during reforging; (2) the remaining larger grains were reduced to several smaller grains during reforging, since they yield at lower stress and deformed and recrystallized more extensively than the finer grains. The exaggerated grain growth in single axis reforgings indicated that activation of additional slip systems and their various interactions during reforging along a second axis were also important in achieving the narrower grain size distribution.

Initial etching studies* indicated faster grain boundary etching in the reforged materials, suggesting greater boundary misorientation, i.e., a more random grain structure in these reforged samples. To date, all forgings exhibited some texture, but generally with substantial grain misorientations (e.g., 20° to 60° arcs were observed on X-ray photographs). As the polycrystalline character and texturing can be affected by temperature, strain, and reforging, studies to delineate these effects are underway.

Crystal Orientation

Chin and Mammel (4) indicate that <111> textures in polycrystalline halides should exhibit higher yield strengths than other textures, since <111> textures result in lower resolved stress on the <100> <110> slip systems. Their study suggests that the press forging of <111> and <110> crystals might alter the resultant polycrystalline texture and hence increase strength. Thus, forging along crystal axes other than <100> were begun.

*The etching techniques consisted of placing the sample in a flowing water bath for 5-10 sec., removal, and after 5-10 sec., rinsing with ethyl alcohol, followed by drying with a warm air gun.

The KCl crystals forged on the <111> and <110> axis at 200°C to 60% strain were free from cracks and edge tearing. The <111> forgings had grain sizes of 10-15 μm and microstructures similar to those obtained with <100> crystals at 200°C, 50% strain (Fig. 4c). The texture in the <110> and <111> forgings will be analyzed in subsequent studies.

Alloyed KCl

Based on the work of Chin et al (5), press forging studies of $SrCl_2$-doped KCl <100> axis crystals were initiated. Crystals of KCl-0.1 m/o $SrCl_2$ (see Section 2.1 and 4.2) were forged to ≈65% strain at temperatures of 210°, 230°, and 260°C using the single stage, single axis forging technique.

The resultant polycrystalline microstructures (Fig. 6) appear to be similar to comparable undoped crystal forgings; however, the recrystallization and grain growth behavior suggest that the $SrCl_2$ increased the recrystallization temperature of KCl. The recrystallization temperatures of metals are known to be affected by impurities, as shown by Clarebrough et al (6). Thus, KCl-$SrCl_2$ forgings at lower temperatures (150° to 200°C) and strains should demonstrate the alloying effects on the recrystallization temperature. Here, thermal calorimetry may be useful in determining recovery and recrystallization temperatures of alloyed KCl and the effects of forging strain and temperature on primary and secondary recrystallization.

Alkaline Earth Halides

Initial press forging of materials for 3-5 μm laser windows centered on BaF_2. These initial studies showed that successful forgings required temperatures of 600°C or greater. Lower temperatures resulted in extensive cracking due to limited plastic flow in these crystals. This study will continue to further develop a polycrystalline microstructure by control of forging temperature and strain and to measure the mechanical properties of polycrystalline BaF_2.

2.2.4. Future Forging Studies

Since point-to-point variations in absorption have been observed in low absorption, high purity KCl forgings (Section 4.2), major concern will center on improving, understanding, and reducing such absorption. IR, Auger, and mass spectrographic analyses of the starting crystals

and the resultant forging will be used to study the effects of the press-forging procedures (atmosphere, etc.) on absorption in conjunction with calorimetric studies. As a result of the Sr-doped KCl study, thermo-calorimetry (differential thermal analysis or differential scanning calorimetry) studies of as-forged materials will be employed to determine recrystallization temperatures, as well as the extent of recrystallization. These techniques should be applicable as controls in the fabrication of large window shapes.

Besides continued efforts in forging alloyed halides and alkaline earth halides, additional work on scaling the size of the windows from a 2" diameter limit up to a 6" limit is in progress. Fabrication of the forging furnace is underway and a large press is available. Also, large 2"x2"x4" KCl crystals are on hand, so that 5-6" diameter window forgings are anticipated in the near future.

1. P. F. Becher and R. W. Rice, "Press Forging Studies" in ARPA Order No. 2031, Semi-Annual Report No. 1, U.S. Naval Research Laboratory (1972).

2. P. F. Becher and R. W. Rice, "Microstructural Influence on the Mechanical Properties of Alkali Halides," to be published in Proc. of High Power Infrared Laser Window Materials, AFCRL (1972).

3. G. E. Bernal, B. G. Koepke, R. J. Stokes and R. H. Anderson, "Preparation and Characterization of Polycrystalline Halides," to be published in Proc. of High Power Infrared Laser Window Materials, AFCRL (1972).

   G. E. Bernal, B. G. Koepke, R. J. Stokes and R. H. Anderson, "Preparation and Characterization of Polycrystalline Halides for Use in High Power Lasers," QTR No. 2, ARPA Order No. AO2172, Honeywell Research Center (1972).

4. G. Y. Chin and W. L. Mammel (1972), "A Theoretical Examination of the Plastic Deformation of Ionic Crystals, II." to be published in Met. Trans.

5. G. Y. Chin, L. G. Van Uitert, M. L. Green and G. Zydzik, "Hardness, Yield Strength and Young's Modulus in Halide Crystals," Scripta Met. 6, 475 (1972).

6. L. M. Clarebrough, M. E. Hargreaves and M. H. Loretto, "Changes in Internal Energy Associated with Recovery and Recrystallization," pp. 63-120 in Recovery and Recrystallization of Metals, L. Himmel, ed., Interscience Publishers, N.Y. (1963).

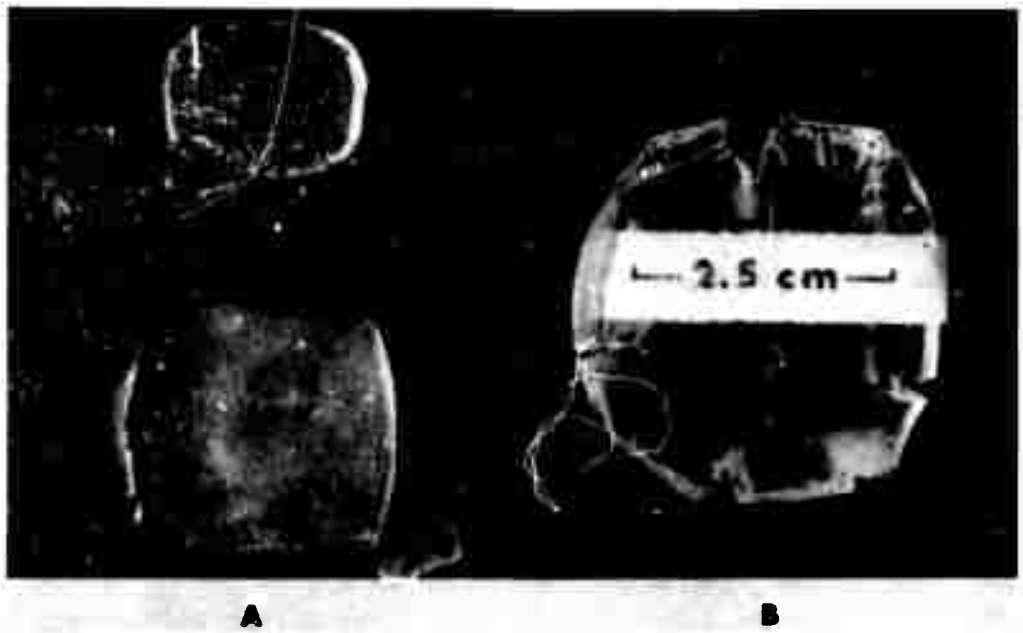

Fig. 1. Effect of End Constraint on KCl Press Forgings. Use of A (top) pyrolytic graphite foil lubricant to relieve end constraint yields rough surfaces, and (bottom) silicone-coated graphite rams minimize surface roughness and relieve end constraints. B. Tearing and fracture resulting from high end constraint forces.

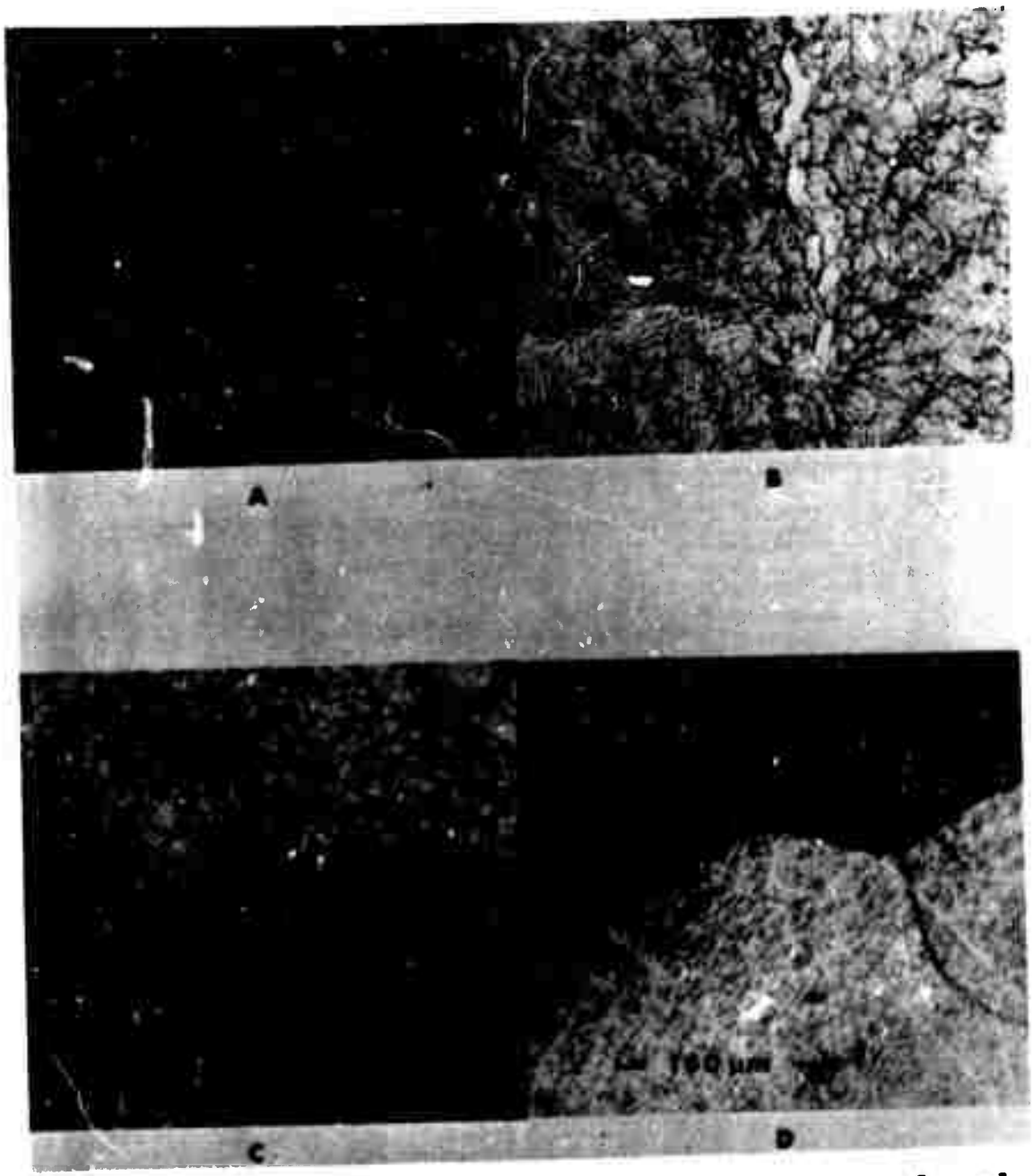

Fig. 2. Microstructure of <100> KCl Crystals press forged at 125°C to different strains. A, 30% strain; B, 40% strain, limited formation of subgrains; C, 50% strain, polycrystalline matrix (~12μm); D, 70% strain, large (~0.3 mm) grains from exaggerated growth.

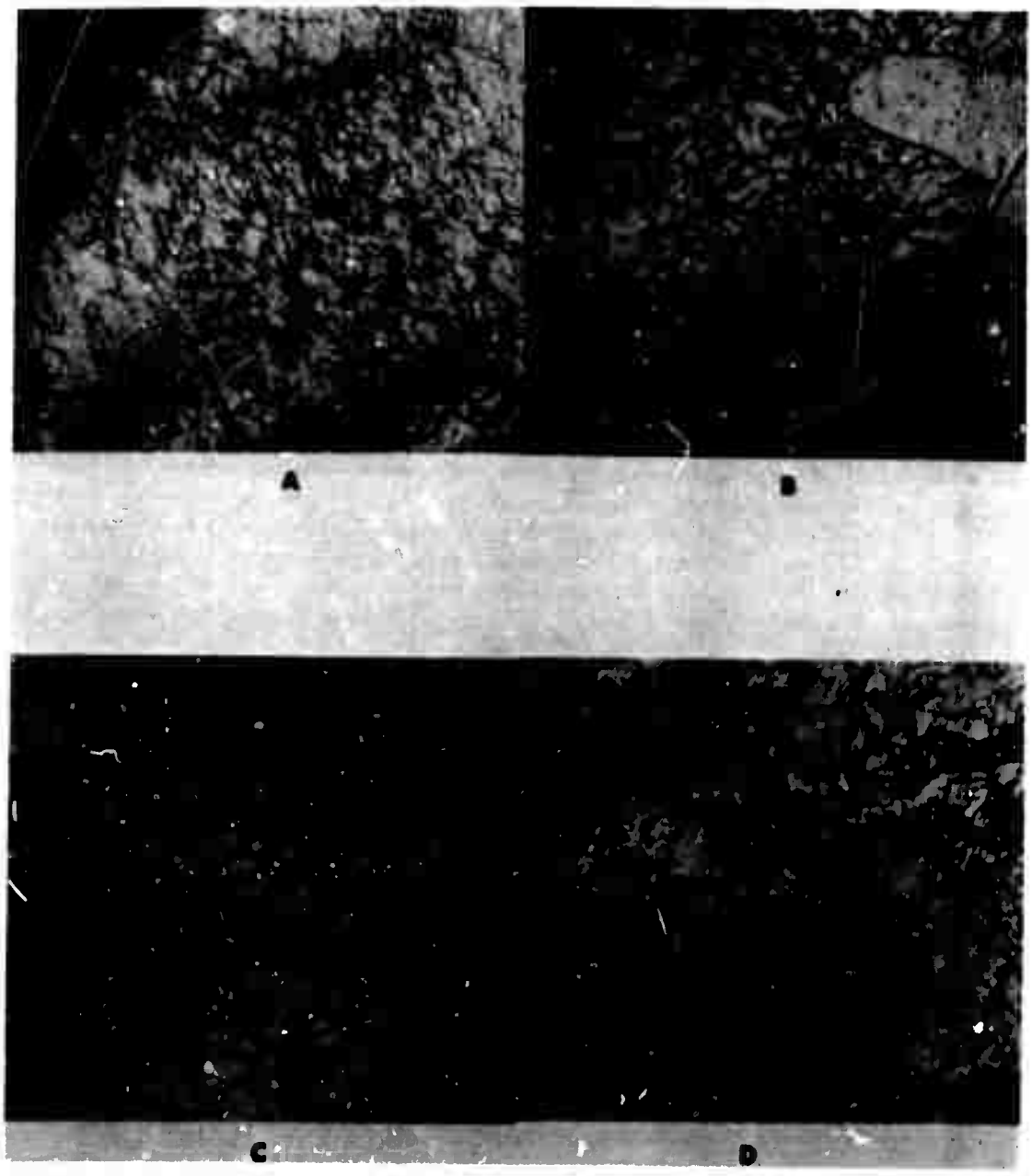

Fig. 3. Microstructure of <100> KCl Crystals press forged at 150°C. A, 30% strain, single crystal with limited sub-grain structure; B, 40% strain, bimodal grain size (15μm/ <100μm); C, 50% strain, fine grained polycrystal (12μm); D, 70% strain, exaggerated grain growth in 15μm grain matrix.

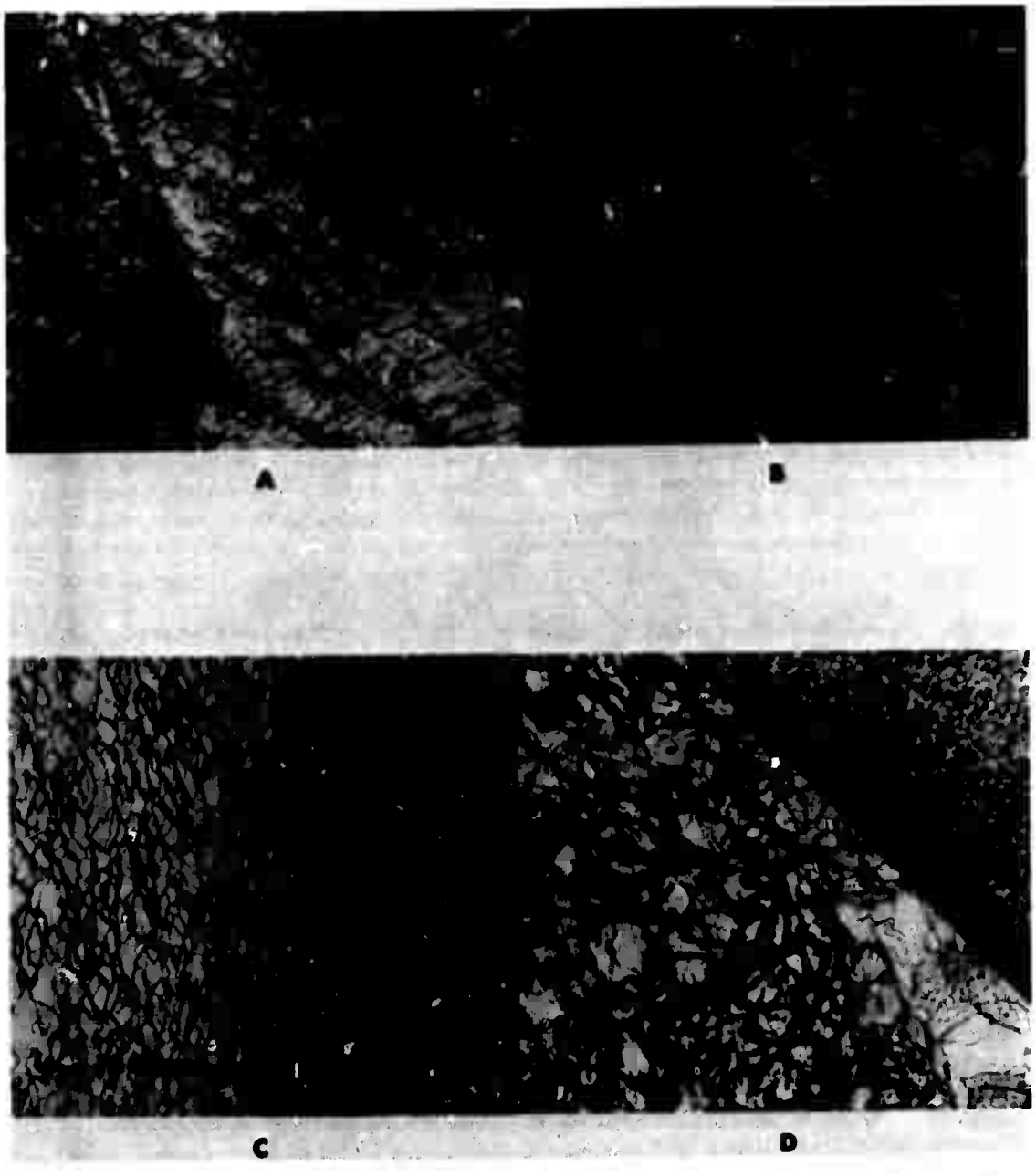

Fig. 4. Microstructure of <100> KCl Crystal press forged at 200°C. A, 30% strain, development of polycrystalline microstructure; B, 40% strain, 13μm grain size polycrystal (large grain at left contains a fracture); C, 50% strain, fine grained matrix (<10μm); D, 70% strain, exaggerated grain growth in 20μm grained material.

Fig. 5. Microstructure of KCl after reforging along new <100> axis to 65% strain at 200°C. A, forged initially at 125°C to 40% strain, 9μm grain size; B, initially forged at 150°C to 40% strain, 9μm grain size; C, forged initially at 200°C to 40% strain, 9μm grain size.

Fig. 6. Press Forged 0.1 m/o $SrCl_2$-KCl. Crystal forged to 65% strain at 260°C; 15μm grain size.

2.3. Chemical Polishing, J. W. Davisson

2.3.1. Introduction

The objective of this work is to develop techniques for producing a high quality surface finish on alkali halide laser windows. A high quality surface must be smooth and flat as well as have low absorption. Such surfaces can probably be obtained using the technique of controlled chemical polishing on flat mechanically polished surfaces. Previous results (1,2) have shown that controlled chemical polishing of NaCl and KCl windows is obtained using hydrochloric acid. There, smooth but not flat surfaces were obtained by prolonged chemical polishing of the mechanically polished surfaces.

A flat chemically polished surface can be obtained in principal from a flat mechanically polished surface if the polish removes only the scratch-containing layers of the surface by means of the surface migration of steps, Fig. 1. The sides of each scratch or abrasive marking consist of steps, hence edges, which are active dissolution sites. Therefore the entire surface will essentially be active in the dissolution process until these active layers are removed. Thereafter, the sides of the piece, which provide a continuous source of edge material, will be the most active and edge rounding will occur. However, the larger the window, the less significant this rounding will be. Thus surface flatness can be naturally preserved if the initial action of chemical polishing involves the surface migration of steps and removes only the first few microns of the surface. Preferential reactivity of steps and only limited surface removal should preclude other polish-surface dissolution such as that associated with stresses that can lead to irregular polished surface.

2.3.2. Results

Since the scratch depth is in the micron range, a dissolution rate in the range of microns per minute is suitable for the controlled chemical polishing of alkali halide windows. An estimate of the dissolution rates of NaCl and KCl crystals in HCl polishes was obtained by measuring with a micrometer the change in thickness (nominally 15 microns) produced by chemically polishing 1 cm^2 cleaved crystals for a known period of time. The specimens were held in the polishing solution with forceps and agitated over a distance of 1 in. at 2 Hertz perpendicular to the face. Dissolution rates of 10, 0.05, and 0.00005 microns/sec were obtained for the agitated NaCl

crystal in HCl polishing solutions consisting of the volume ratios HCl/H_2O = 0/1, 3/1, and 1/0, respectively. The dissolution rates were reduced by a factor of 5 when the crystals were not agitated. Agitation of NaCl in the 3/1 ratio solution is suitable, since it removes a micron in an easily controlled time of about 20 sec. Agitation of KCl crystals in concentrated HCl (volume ratio = 1/0), which yielded the rate 0.2 microns/sec, is suitable for readily controlled polishing of KCl windows.

The method of prior surface preparation was found to influence the action of the chemical polish on NaCl. Thus a smooth surface was produced ab initio by the polish when the surface preparation involved sanding, but not when it involved lapping. In the latter case, however, a smooth surface was obtained immediately by the polish after the crystals were annealed 30 minutes at 600°C. The mechanical operations of sanding and lapping used to prepare these surfaces were carried out as follows. For the sanding operation, each of three 1 cm^2 beveled cleavage specimens of NaCl was waxed to one end of a 400 gram 1" dia. steel rod having free vertical motion in a hand-held collet, then abraded by sanding over a distance of 12" in the [100] crystal direction, first against No. 400 and then against No. 600 wet or dry tri-m-ite (3M) silicon carbide paper. For lapping each of three beveled specimens was waxed to a 50 gram 1" dia. brass disc, then rubbed with a circular motion on glass plate covered with a No. 7 emery grit-isopropyl alcohol slurry. Both types of surfaces were then hand-polished using Linde A and isopropyl alcohol on polishing cloth.

The distinction between the two methods of surface preparation is that with sanding, the abrasive particles are rigidly held and the surface is removed by scratching or chipping. In lapping, the abrasive particles are free and the material is removed under conditions of pressure contact with rolling irregular particles. Because chipping is a manifestation of the damage-free actions of cleavage and fracture, the surface is probably less damaged when it is sanded than when lapped. Thus the sanding operation probably retains the greater surface crystallinity as is manifested by the action of the chemical polish.

The effect of various finishes on NaCl is shown in Figs. 2-5. Figure 2A shows a diffuse layer of dislocation damage from sanding in the [100] direction of about 50 microns, as revealed by etching on transverse faces cleaved perpendicular and parallel to the sanding direction.

After a 30 sec. chemical polish, a smooth surface interlaced with expanding abrasive markings, most of which were not observed on the initial mechanically polished surface, was found as shown in Fig. 2B. After chemically polishing for 90 sec., the features associated with the mechanical polish were virtually eliminated, but there emerged a persistent background structure parallel to the [100] sanding direction (Fig. 2C) and hence is attributed to the sanding operation. Thus, although a smooth surface was obtained ab initio by the polish, a flat surface was not obtained owing to the existence of subsurface structure in such an unannealed crystal. Figure 3 shows that the damage introduced by lapping was localized within a depth of about 30 microns. Figures 4 and 5 compare the action of the chemical polish on the lapped and mechanically polished NaCl crystal before and after it was air-annealed 30 min. at 600°C and then slowly cooled. These views show that a smooth surface was obtained ab initio only after heating the crystal. Presumably, the heat treatment relaxes the elastic stresses and produces recovery of the dislocation damage.

A rigorous study of surface flatness has not been undertaken, but when the surfaces of six chemically polished 1 cm^2 KCl specimens were scanned with a Zeiss interference microscope, no change in the straight line regular interference patterns was observed. These specimens were initially a set of machine-polished flat crystals. The excellent mechanically polished surfaces showed uniform abrasive markings. After chemically polishing for 15 sec., these surfaces were rendered smooth. It is clear that the degree of flatness that can be conserved depends upon the quality of the mechanical polish. The best surfaces for chemical polishing are probably those such as the above which contained a multitude of fine, equally deep, parallel scratches or abrasive markings. Individual deep scratches are detrimental because they become enlarged and are not removed in the short polishing time required to conserve flatness.

To demonstrate the applicability of chemical polishing to polycrystalline KCl, pressed forged samples were polished. Figure 6 shows the degree of smoothness that can be achieved by a 15 min. chemical polish of a press forged KCl (80% reduction) specimen that was annealed for one hour in Argon at 100°C. A prolonged chemical polish was used in this instance to obtain the steady state configuration of the polishing surface, but the same configuration was obtained after only a few minutes of polishing.

This smooth surface showed no irregularity and appeared flat except within a 1μ-wide region at grain boundaries where grooving occurred.

A high quality laser window must also show a low optical absorption to laser light. The optical absorption of a chemically polished high purity Hughes KCl crystal, about 2.5 cm thick, to CO_2 laser light was measured calorimetrically. As discussed in Section 4.2., this sample showed a fractional power absorbed of 0.001-0.002, which implies an absorption coefficient, $\beta \leq 0.0006\text{-}0.0008\ cm^{-1}$. Here, only an upper limit of the absorption coefficient is given as no measurements were obtained as a function of length. Comparable absorption values were obtained with a press forging of this single crystal (Section 4.2). It is reassuring to note that both these upper limit values are among the lowest absorption coefficients for KCl that have ever been reported. This strongly suggests that the chemical polishing procedure (1,2) produces surfaces that are not only smooth but also have extremely low absorption.

2.3.3. Conclusions and Future Plans

This work has demonstrated that the technique of chemical polishing shows promise as a way to produce a high quality surface finish on alkali halide laser windows, since the requirements of smoothness, flatness, and absorption can apparently be satisfied. These requirements can probably be simultaneously satisfied by using the chemical polish to remove only the superficial scratch-containing surface layers from flat, mechanically polished, and annealed windows.

Future plans include the further evaluation of chemical polishing with emphasis on surface absorption and a study of the stress fields and dislocation damage introduced by the mechanical processing of alkali halide windows.

1. J. W. Davisson, "Chemical Polishing," p. 22, High Energy Laser Windows, Semiannual Report No 1, ARPA Order 2031, Naval Research Laboratory, Washington, D.C., June 1972.

2. J. W. Davisson, "Chemical Polishing of NaCl and KCl Crystals," to be published in Proc. High Power Infrared Laser Window Materials Conference, Hyannis, Mass., October 1972 (AFCRL).

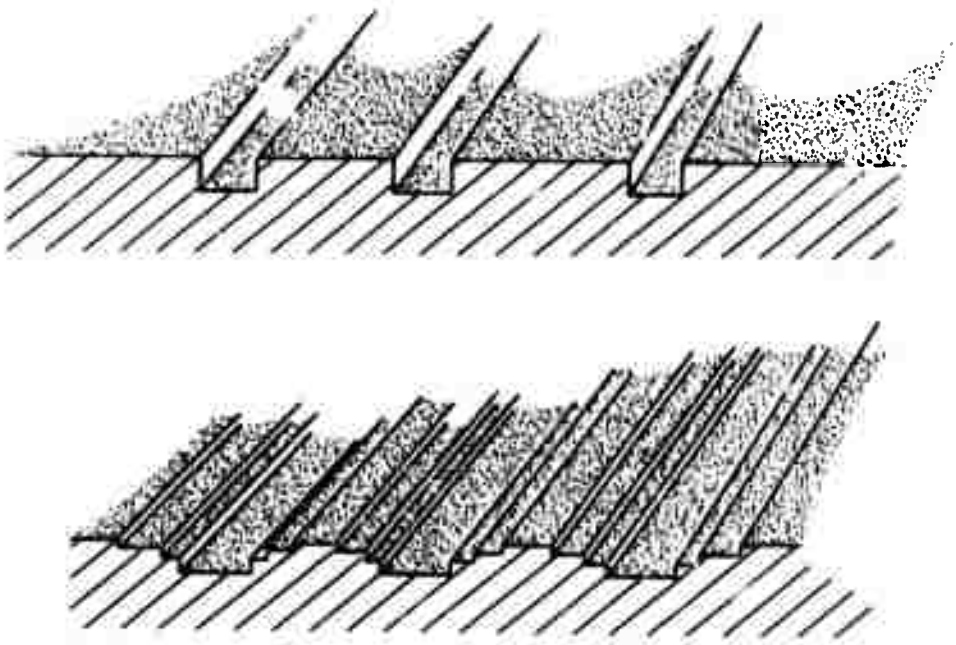

Fig. 1. Removal of Scratches by Polishing Action. The walls of the scratches shown at the top are removed by the stepwise migration of atomic layers as shown at the bottom. A smooth surface is obtained at a later stage of polishing when more of the stepped material has been removed.

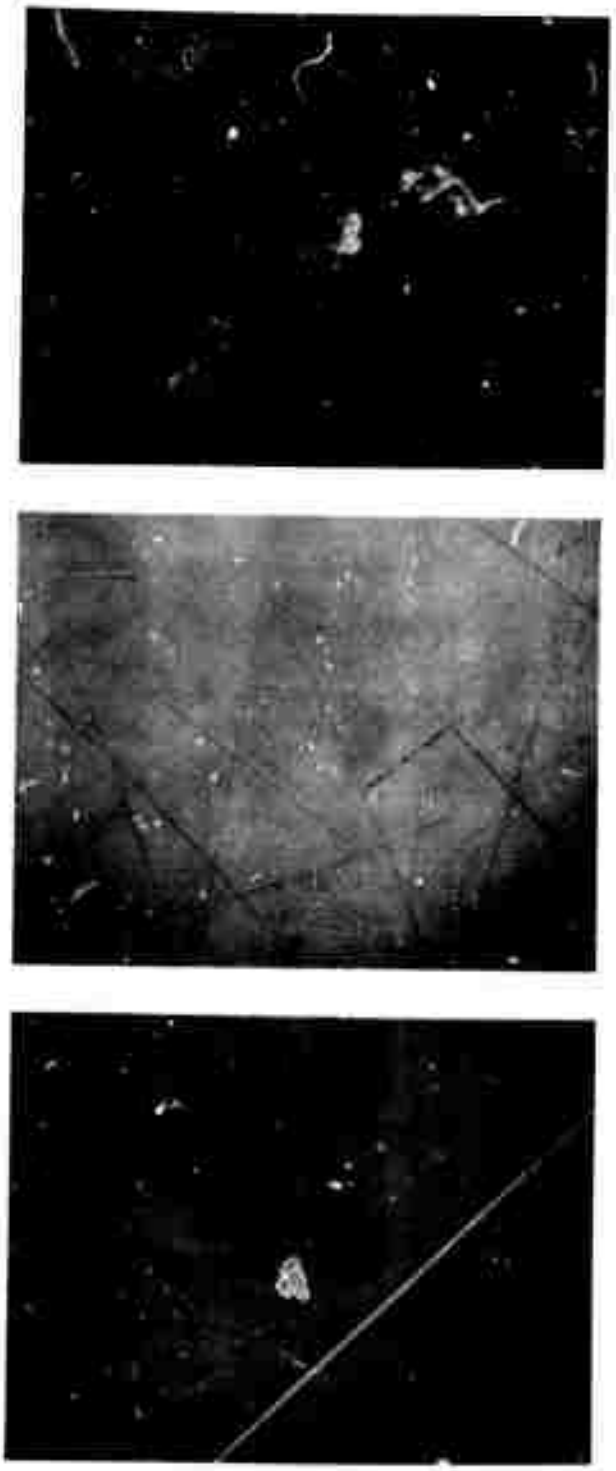

Fig. 2. Unannealed NaCl Window. Top: Dislocation damage due to sanding in [100] direction (X100). A. upper: transverse face perpendicular to sanding direction; lower: transverse face parallel to sanding direction. B. chemically polished 30 sec. (X30). C. chemically polished 90 sec. (X30).

Fig. 3. Dislocation damage due to lapping - transverse cleavage face (X150).

Fig. 4. Unannealed NaCl Window (X45). A. lapped and mechanically polished; B. chemically polished 10 sec.; C. chemically polished 5 min.

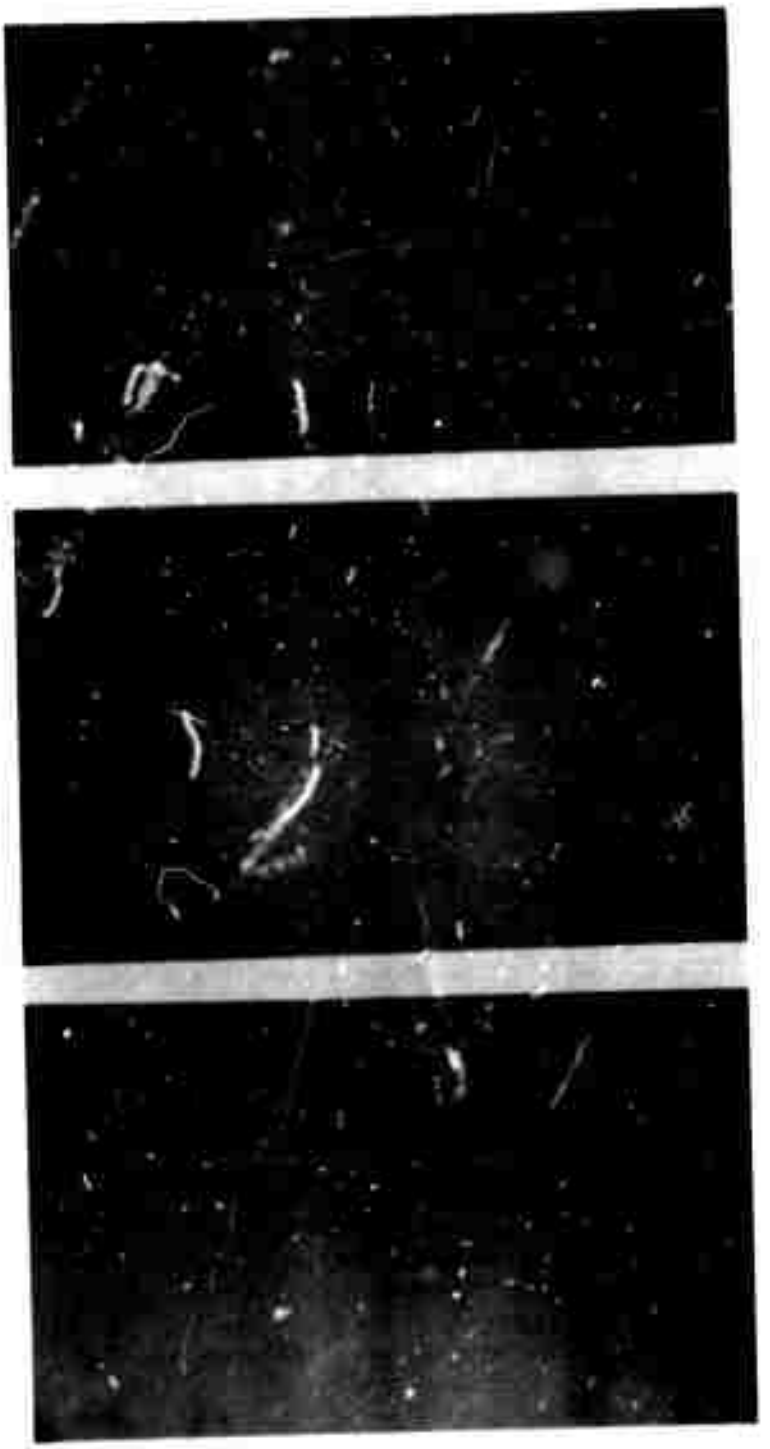

Fig. 5. Annealed NaCl Window (X45). A. window shown in Fig. 3 annealed 30 min. at 600°C and mechanically polished; B. chemically polished 10 sec.; C. chemically polished 5 min.

Fig. 6. Chemically Polished Press Forged KCl Surface Viewed with Scanning Electron Microscope. Surface tilted 45° to beam axis: Top, (50X); bottom, same region (1000X).

3.0. STRENGTH AND FRACTURE OF SINGLE AND POLYCRYSTALLINE KCl, P. F. Becher and S. W. Freiman

3.1. Introduction

The major goal of this study has been to raise the yield strength of alkali halides to 6000 psi or greater without degrading their optical properties. As the yield and fracture behavior of alkali halides are controlled by dislocation motion, strengthening must be achieved by limiting slip processes. The present polycrystalline approach to strengthening is based on Petch-type behavior of the yield stress of the alkali halides:

$$\sigma_y = \sigma_o + kd^{-1/2} \qquad (1)$$

where σ_y is the polycrystalline yield stress, σ_o is the single crystal yield stress, d the polycrystalline grain size, and k, a materials constant. As seen in Table 1, a logical sequence of strengthening techniques can be obtained based on the terms in the Petch equation. First, the term $kd^{-1/2}$ reflects an increased plastic flow resistance from the presence of grain boundaries and raises the strength of polycrystals above that in single crystals. Thus, reducing the grain size (d) offers a means of significantly increasing the yield stress. This grain size refinement technique has previously been shown to raise the yield strength to 5000 psi in fine grained polycrystalline KCl forgings (1,2). The next steps have been to look at alloying and texture effects on strength as they can increase either the σ_o or k terms in Eq. 1. As an example, Chin et al (3) demonstrated that a few hundred parts per million of divalent cation increased the KCl single crystal yield stress (σ_o) from 200 psi to 1000-3000 psi. Increasing the σ_o term would result, of course, in increasing the polycrystalline yield strength, per Eq. 1.

Table 1

Strengthening Technique	Strengthening Effect
1. (a) Develop pore-free polycrystal	Gain $\left(+ kd^{-1/2}\right)$
(b) Refine grain size	Increase $d^{-1/2}$
2. Alloyed polycrystal	Increase σ_o
	Increase k
3. Preferred orientation (a) Type	Increase or Decrease σ_o
(b) Degree	Increase or Decrease k

An important tenant of this program has been that fracture energy or toughness, as well as strength, is an important criteria for avoiding window failure. Fracture energy could, for example, control failure under conditions of repetitive stress of limited duration or spatial extent which could only cumulatively lead to failure. Concern for increasing fracture energy to avoid fracture was another factor in selecting the polycrystalline approach. Based on the study of MgO by Evans (4), polycrystalline halides were expected to be substantially tougher (~tenfold) than single crystals.

3.2. Experimental Technique

The single crystal specimens used in both yield stress and fracture energy measurements were cleaved from bulk crystals generally followed by water polishing on billiard cloth. They were given a finish polish by dipping them into a water bath and immediately rinsing with ethanol and drying in warm air. Polycrystalline samples were cut from forged disks with either a wire saw or a 10-mil rubber-bonded 180-grit alumina cutoff wheel using an isopropanol coolant, then water-polished.

Slotting and grooving of all fracture energy specimens was done prior to water-polishing with the same cutoff wheel technique employing about a 20-mil depth of cut per pass at feed rates of 2 in/min. For fracture energy measurements, the single crystal samples were then annealed at 300°C for 3 hrs., and the polycrystalline

specimens annealed at 100-125°C for 3 hrs. After annealing, all specimens were kept in a desiccator until tested.

Yield strengths were measured with flat bar specimens using three point bending on spans of 0.35 and 0.50 in. at cross head speeds of 5×10^{-2} in/min (outer fiber $\dot{\varepsilon}$ $2\text{-}4\times10^{-2}\text{in}^{-1}$) at ≈22°C in 40-50% relative humidity. The yield strength was taken as the proportional limit (i.e., the point where the stress-strain curve becomes nonlinear).

Fracture energy and crack growth studies were undertaken using an NRL-developed (5) modification of the widely used double-cantilever-beam technique. The modification consists of applying a moment to the specimen by means of lever arms (Fig. 1) instead of applying a force normal to the crack directly to the arms. The primary advantage of applying a moment is that the energy available for the extension of a crack is independent of its length, thereby facilitating crack growth investigations. In addition, no contributions to fracture energy due to shear or beam rotation occur, while these effects must be corrected for in other double cantilever configurations. The strain energy release rate, $\mathcal{G}$, for this arrangement is given by

$$\mathcal{G} = 2\gamma = \frac{M^2}{EIt} \qquad (2)$$

where γ is the fracture energy, M is the moment applied to the arms attached to the sample, E is Young's modulus of the specimen, I is the moment of inertia of one side of the specimen about its longitudinal axis, and t is the specimen thickness at the center groove used to guide the crack. The moment is determined by the product of the force applied to a lever arm and the distance from the point of load application to the fulcrum of the arm. Studies of crack growth at constant $\mathcal{G}$ were carried out by applying a constant force to the arms by means of a closed loop test machine via the linkage shown in Fig. 2. A given load is produced by means of a potentiometer. The output of a load cell is amplified and fed into an electrohydraulic servo controller of ram displacement*, which keeps this load constant. The output of the load cell is also fed, after amplification and scaling, into a digital voltmeter, allowing the experimenter to directly observe the force on the lever arms.

* Moog Corporation

Fracture energy specimens (Fig. 1), 1-2" long, consisted of crystals with the center groove parallel to a <100> to propagate {100} cleavage cracks and polycrystalline bars with the crack propagation groove placed such that it corresponded to the central region of the original forged disk and was parallel to the disk surface. The specimens were affixed to aluminum loading arms with epoxy cement which was air-cured at 70°C for 3 to 4 hours. Just before testing, a sharp crack was initiated at the top of the sample by tapping with a razor blade to insure measurement of accurate fracture energies. The specimen was then inserted into the loading rig, as shown in Fig. 2. All testing was performed in air at 22°C and 50% relative humidity. The test procedure involved slowly increasing (10-20-gms/min) the load on the sample while observing the crack tip in a travelling microscope. Because of the slow loading rate, the applied load at which the crack propagated could be determined to ±1 gram. At intervals, the load was held constant for a time to investigate the possibility of slow crack growth.

3.3. Results and Discussion

3.3.1. Yield Behavior of Polycrystalline KCl

Previous results have shown the effect of decreasing grain size of KCl on the room temperature yield stress (1,2) following the Petch equation, as shown in Fig. 3. The yield stresses from other studies show excellent agreement with the present work, despite differences in specimen sizes and test methods. These data of Grant (6), Wurst (7), and some of Harrison et al (8), were obtained in four point bending and all data are for different strain rates. Data from Bernal et al (9) in three point bending also substantiate the authors' results.

Limited data for <111> KCl forgings indicate either an increase in the slope (k) of yield strength versus (grain size)$^{-1/2}$ or an overall upwards shift in the strength. This increase in k is expected if the misorientation between grains increased while the overall increase in strength reflects higher σ_o or single crystal yield strength. The latter is espected, as <111> crystals exhibit higher yield strengths than <100> crystals and the polycrystalline bodies may have comparable textures as discussed by Chin and Mammel (10). A cooperative increase in both k and σ_o cannot be ruled out until further texture studies are completed.

The initial polycrystalline KCl-0.1 m/o $SrCl_2$ yield strength data (Fig. 3) show a substantial increase over "pure" KCl bodies. Both the σ_o and k Petch terms are increased by alloying as expected. These materials illustrate that incorporation of divalent cations in press-forged polycrystalline KCl can result in yield strengths of at least 6000 psi. Present studies are involved with the effects of Sr level on the forging behavior and resultant yield strength of KCl. Lower Sr levels might still have significant strengthening effects and result in low absorption values.

The plastic strain associated with yielding was ~0.01% prior to fracture in as-forged materials. However, as noted in Section 2.2, low temperature anneals resulted in a tenfold increase in strain without affecting grain size or yield stress sericusly. The fracture stresses of as-forged KCl approached 6000 psi in fine-grained materials, decreasing to 2000-3000 psi in large-grained bodies. Fracture occurred primarily by transgranular cleavage and appeared generally to initiate in the largest grains on the tensile surface.

3.3.2. Fracture Energy

Single Crystals

The fracture energies of both the single crystal and polycrystalline KCl were calculated using Eq. 2 with a value of $E = 5.6 \times 10^6$ psi. Single crystal results (Table 2) show that the fracture energies of the single crystals in which the specimen thickness at the crack, t, is fairly small (<.05") are high compared to the value of 110 ergs/cm^2 determined by Westwood and Goldheim (11). The plastic zone size, r, in these specimens was calculated using Eq. 3 (12).

$$\gamma = \frac{\mathcal{J} E}{2\pi\sigma_y^2} \qquad (3)$$

where σ_y is the yield strength of KCl. Taking σ_y = 600 psi (1), one obtains a value of r of .02 to .03", giving a ratio of thickness to zone size of from 1 to 2. In practice, a ratio of from 6 to 10 is required to produce a state of plane strain. If the crack tip is in a state of plane stress, the plastic region extends to a free surface, allowing additional elastic energy to be absorbed in slip, thereby increasing the driving force needed for crack growth. When specimens of the required thickness

were tested (K9 and K10), values of γ close to that expected were attained. Similar effects of plane stress and plane strain testing were observed in NaCl by Wiederhorn (13). Remaining differences between the energies measured in this study and those reported by Westwood and Goldheim (11) could be due to differences in purity of the KCl and humidity during testing. In addition, these values may be slightly high due to the small amount of plastic deformation in the specimen arms. In both K8 and K9, the reported γ's are those which first caused the cracks to jump forward to new positions. Greater loads were required to propagate the arrested cracks completely through the crystals. No slow crack extension was observed.

Press-Forged KCl

The fracture energies of the polycrystalline press-forged KCl (Table 1) ranged from 600 ergs/cm^2 to approximately 3400 ergs/cm^2. The average fracture energy of press forged KCl was about 2000 ergs/cm^2, an order of magnitude greater than that of the single crystals, as expected. The stress conditions in the polycrystalline KCl probably lies intermediate between plane stress and plane strain, depending on the yield stress of the specimen. This value could vary between 3000 to 5000 psi for these specimens, giving rise to a plastic zone size in the approximate range .006" to .017". This variance could be one of the main factors producing the scatter in results. These thinner samples were used because of the difficulty in obtaining thicker ones in the length and width needed in the test.

No slow crack growth was observed in the press-forged KCl. In fact, one sample was held for 48 hrs. at 75% of the failure load with no visible change in crack position. It was seen, however, that a damage zone sometimes existed at the crack tip during loading. This zone appeared to consist of a large number of small flaws radiating out from the primary crack and could serve to increase the energy necessary to propagate it (14). Because of the easy cleavage of individual grains, such behavior is not unexpected. The tendency of the crack to veer out of the groove during propagation is probably also related to the existence of flaws along the groove edges which can propagate due to the bending moment in the arms.

Microstructure and Fracture Topography

The SEM micrograph of a water-etched surface of press-forged KCl, shown in Fig. 3, indicates a fairly wide grain size distribution (2 to 15μ). An average grain size of 6μ

was determined by quantitative microscopy. No significant variation in the grain size distribution among the samples was observed.

The fracture surfaces of the press forged specimens varied from large flat areas of cleavage (Fig. 4) to areas containing a fair number of cleavage steps, such as shown in Fig. 5. This latter micrograph indicates the presence of grain misorientation, as evidenced by the ripple-like structure on the cleavage faces.

3.4. Summary

Alloying with limited (e.g., 0.1 M/o or less) of divalent ions and possibly texturing increases strength. The σ_o and k terms of the Petch equation are clearly increased by alloying and possibly by texturing. Irradiation hardening, which is being studied, can also increase strengths of press-forged bodies. Clearly, combining one or more of these techniques with press forging will give yield strengths over 6000 psi. These supplemental strengthening techniques should be more important in larger forgings where microstructure variations may result in somewhat lower yield stresses (e.g., 3000-4000 psi), than the approximately 5000 psi achieved in laboratory specimens.

Using a modification of the double-cantilever beam test, the energy required to repropagate a sharp crack was found to increase from about 230 ergs/cm^2 for single crystals to approximately 2000 ergs/cm^2 for press-forged materials having an average grain size of about 6μ. No evidence of slow crack propagation was noted in either case, although a damage zone was observed at the tip of cracks in the polycrystalline specimens. Scanning electron microscopy showed that the fracture surfaces of the press-forged samples were very rough compared to the flat {100} cleavage faces of the single crystals. Although there were fairly extensive cleavage faces in these samples, evidence of grain misorientation could be seen through its effect on fracture roughness. This misorientation is probably one of the main factors leading to the increased fracture energy of these specimens.

3.5. Future Plans

Further supplemental strengthening will be sought by low levels of divalent alloying, texturing, and/or irradiation. While these types of forgings may have somewhat lower fracture energies (toughness) than the KCl forgings

studied above (3.3.2), any forged polycrystalline body should be tougher than its parent single crystal. Therefore, fracture energy will be studied in polycrystalline KCl in terms of microstructure (grain size and grain misorientation effects) along with texture, irradiation, and alloying effects in single crystals and polycrystalline bodies.

An attempt will be made to use acoustic emission techniques in fracture energy tests to predict the load at which a crack will be propagated. Other factors such as environment and loading rate will also be considered in future fracture testing. The latter may be especially important since stresses incurred in KCl windows due to laser heating effects should be dynamic in nature. Similarly, strain rate and temperature effects on the yield strength of polycrystalline halides will be studied to predict their yield behavior in a laser system.

To test these results, windows of press-forged KCl* will be tested in a laser system to study the effect of irradiating these materials. Initial testing of these samples is to be done in a lower power (0.3 KW) CO_2 laser with a CW beam. Analysis will include beam-induced damage using birefringent effects to observe local strains, beam heating using thermal couples and other temperature-sensing techniques, and post-irradiation microscopy of window surface for evidence of damage. Subsequent tests will include use of these windows in the NRL-CBD laser system where failure of single crystal KCl windows has occurred. These tests will be concerned mainly with life expectancy of the polycrystalline windows and laser damage. Future studies are to include higher power level laser testing in conjunction with current NRL studies on laser damage in materials.

*At present, 1.5" diameter windows are being machined from forgings in a lathe using a conventional cutting tool. To remove material from the circumference of the forging and avoid cracking and edge chipping, a low cutting angle (~15°) was maintained between the tool cutting surface and the window surface. These samples are then strain relief annealed at 100°C for 3-4 hrs. and the disk surfaces given a final mechanical polish, followed by a chemical polish.

1. P. F. Becher and R. W. Rice, (1972), "Press Forging Studies" in Semi-Annual Report No. 1, ARPA Order No. 2031, U. S. Naval Research Laboratory.

2. P. F. Becher and R. W. Rice, (1972), "Microstructural Influence on the Mechanical Properties of Alkali Halides," to be published in Proc. of High Power Infrared Laser Window Materials, AFCRL.

3. G. Y. Chin, L. G.Van Uitert, M. L. Green and G. Zydzik (1972), "Hardness, Yield Strength and Young's Modulus in Halide Crystals," Scripta Met. 6, 475.

4. A. G. Evans, (1970), "Energies for Crack Propagation in Polycrystalline MgO," Phil. Mag. 22, 841.

5. S. W. Freiman, D. R. Mulville and P. W. Mast, "Crack Propagation in Ceramics," Report of NRL Progress, Feb. 1972.

6. N. J. Grant, (1972), "Research on Materials for High Power Laser Windows," QTR No. 1, ARPA Order No. 2055, Massachusetts Institute of Technology.

7. J. C. Wurst (1972), "Characterization of the Flexural Strength of Polycrystalline KCl," Report UDRI-TM-72-04, University of Dayton Research Institute.

8. B. W. Harrison, G. Hendrickson and J. Starling (1972), "Halide Material Processing for High-Power, Infrared Laser Windows," Interim Report No. 1, Contract No. F-33615-72-C-2019, Honeywell Corporation.

9. G. E. Bernal, B. G. Koepke, R. J. Stokes and R. H. Anderson (1972), "Preparation and Characterization of Polycrystalline Halides for Use on High Power Lasers," QTR No. 2, ARPA Order No. A02172, Honeywell Research Center.

10. G. Y. Chin and W. L. Mammel (1972), "A Theoretical Examination of the Plastic Deformation of Ionic Crystals, II," to be published in Met. Trans.

11. A. R. C. Westwood and D. L. Goldheim, (1963), "Surface Energy of {100} Potassium Chloride," J. Appl. Phys. 34(10), 2085.

12. G. R. Irwin, "Properties of Crystalline Solids," ASTM Publication STP 283 (1960).

13. S. M. Wiederhorn, R. L. Moses, and B. L. Bean, "Plastic Deformation and the Fracture Surface Energy of Sodium Chloride," J. Am. Ceram. Soc. 53(1), 18 (1970).

14. R. G. Hoagland, et al, "Influence of Microstructure on Fracture Propagation in Rock," Final Report, Battelle, Columbus Laboratories, ARPA Order No. 1579, Jan. 1972.

Table 2

Fracture Energies of KCl

Specimen No.	Condition	Specimen Dimensions (in.) w	t	h	γ (ergs/cm^2) (1)	Observations
K1	Single Crystal	.11	.050	.13	740	Great deal of plastic deformation of specimen arms.
K2	Press Forged	.063	.029	.11	>1600	Fractured when specimen arms broke.
K3	Press Forged	.059	.030	.19	1850	Crack propagated at ≈45° angle to groove.
K4	Press Forged	.070	.040	.23	>1000	Fractured when specimen arms broke.
K5	Press Forged	.071	.040	.23	3400	Lot of damage visible at crack tip. Crack propagated out of groove.
K6	Single Crystal	.065	.024	.24	850	No plastic deformation of arms observed.
K7	Single Crystal	.068	.035	.24	1050	Crack propagated down groove and arrested.
K8	Single Crystal	.084	.048	.24	670	No plastic deformation of arms observed

(continued)

(continued)
Table 2
Fracture Energies of KCl

Specimen No.	Condition	Specimen Dimensions (in.) w	t	h	γ (ergs/cm^2)(1)	Observations
K9	Single Crystal	.245	.245(1)	.25	225	Crack arrested after propagating. Small amount of plastic deformation in arms.
K10	Single Crystal	.246	.246(1)	.25	230	Crack arrested after propagating. Small amount of plastic deformation in arms.
K11	Press Forged(2)	.058	.026	.24	600	Crack propagated down groove.
K12	Press Forged(2)	.067	.026	.24	>3300	Specimen broke while attempting to lengthen crack.

(1) No groove.
(2) Hughes' KCl starting crystals.

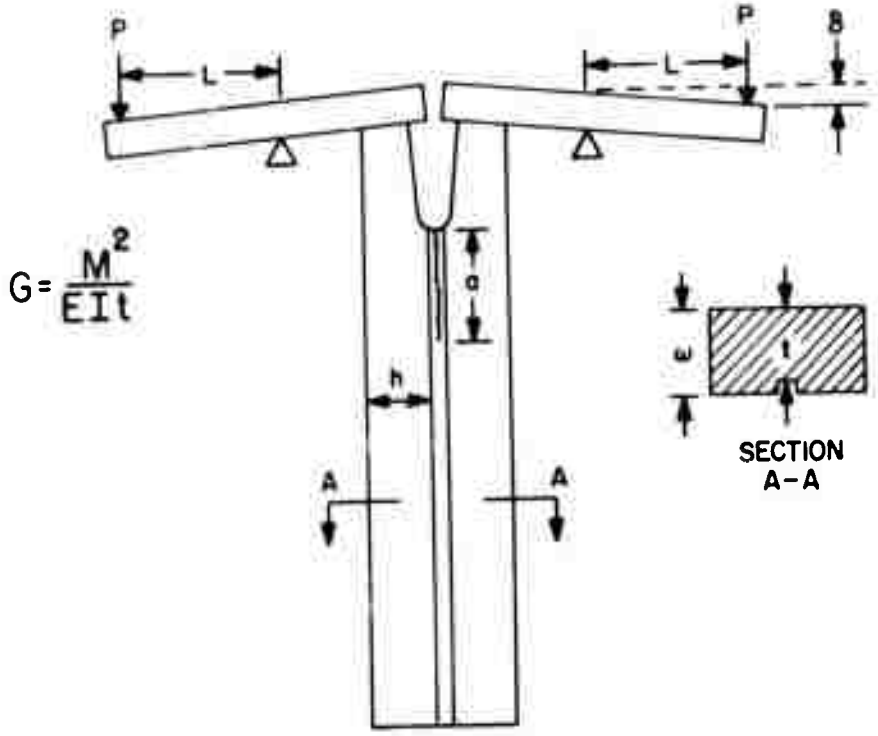

Fig. 1. Schematic of specimen for fracture energy measurements by a modified double cantilever beam test.

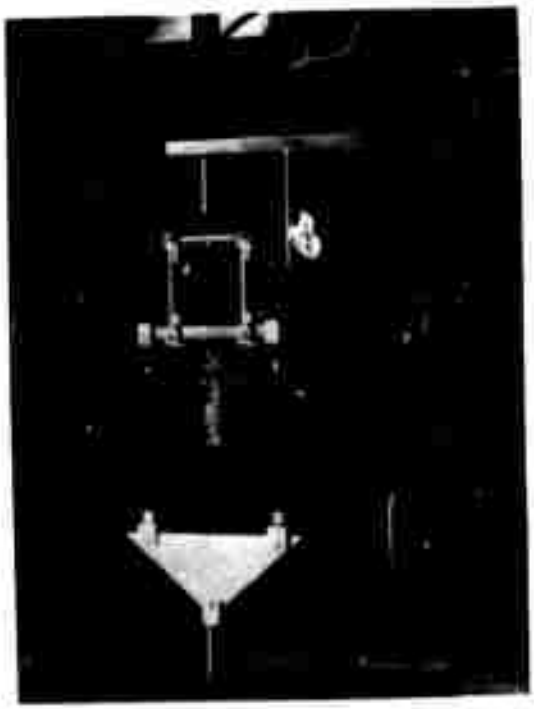

Fig. 2. Fracture energy specimen in load train of a closed loop test system.

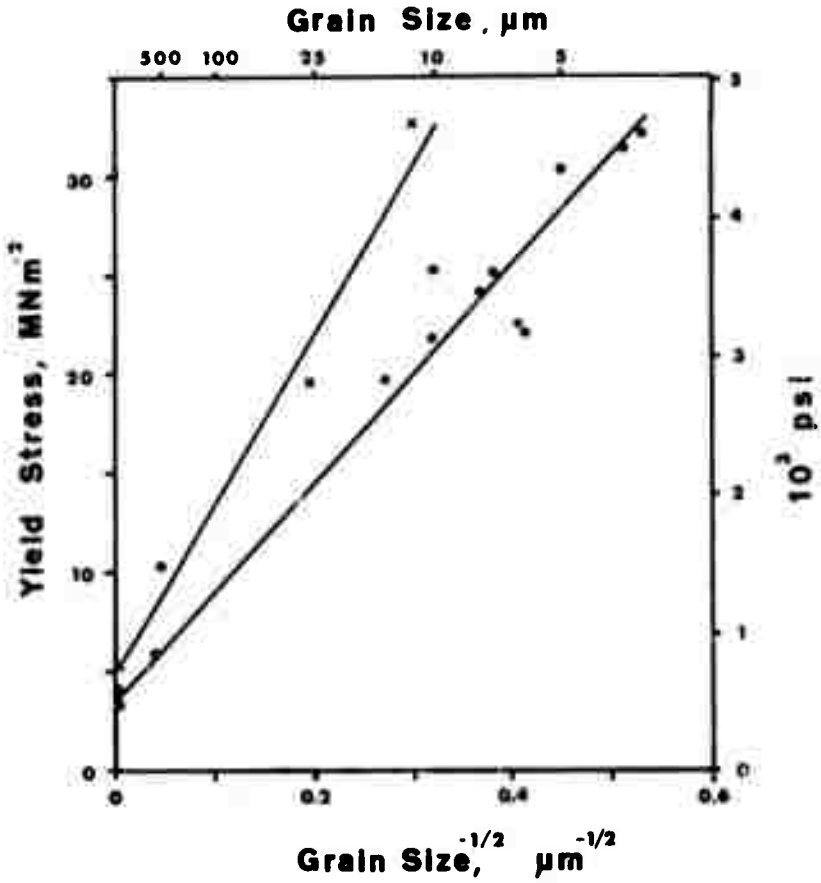

Fig. 3. Grain size dependence of yield strength in press-forged KCl materials (●- pure, <100> forgings, o - pure, <111> forgings, and x - 0.1 m/o $SrCl_2$ doped, <100> forgings).

Fig. 4. Polycrystalline microstructure of test specimen K5 polish surface illustrating its fine grain structure.

Fig. 5. Large Cleavage Area on fracture surface (specimen K4).

Fig. 6. Variation in Cleavage Surface (banded structure) associated with grain misorientation.

4.0. OPTICAL ABSORPTION STUDIES AT 10.6μm

Investigations of the optical absorption at 10.6μm are in progress as part of the laser window effort. The principal objectives of this effort are the following:

(1) Techniques of laser calorimetry: development of methods, establishment of validity of approach, and specific heat determination using methods of laser calorimetry.

(2) Surface absorption diagnostics: relation between chemical polishing and surface absorption.

(3) Absorption of press-forged materials and single crystals: relation between absorption of starting single crystal and final press-forged material.

(4) Temperature dependence of absorption in single crystals: emphasis on showing a different temperature dependence of absorption associated with impurities and intrinsic origin.

(5) Absorption of single crystals subject to strengthening procedures: relation between absorption and strengthening by divalent doping and irradiation.

In this effort, the first item listed above has essentially been completed as is described in detail in this report. The second item concerning surface absorption is a continuing effort in conjunction with the polishing studies (Section 2.3). Preliminary results are reported here showing that the surface absorption for chemically polished KCl crystals is very low. Quantitative data will be forthcoming in the future. The details of the absorption of press forged materials are discussed in greater detail here as the results preclude quotation of a single number for the absorption coefficient. The fourth item, relating to studies of the temperature dependence of the absorption in single crystals, has been stimulated by recent theoretical analyses (Sec. 5.0). This work is in its initial phase and will not be discussed further here. Potentially, this is of great significance both because of intrinsic theoretical interest and because it might provide a straightforward way of distinguishing between intrinsic and impurity absorption as indicated in the theoretical section. Finally, some measurements on irradiated crystals have been initiated with a view towards showing if there are any absorption changes in irradiation crystals. This work is in its initial stages and will be reported at a future time.

4.1. Calorimetry, M. Hass and F. W. Patten

4.1.1. Introduction

Laser calorimetry is well established as a method of measuring the low levels of absorption existing in infrared laser window materials. The "adiabatic" technique developed by Horrigan and Rudko (1) at Raytheon has been adopted by most investigators in this field. Basically, the temperature of a sample thermally isolated from its surroundings is measured as a function of time. When a laser beam of constant intensity is incident on the sample, energy will be absorbed at a constant rate resulting in a linear rise in temperature to a first approximation.

In this present report, a way of establishing the validity of this method by use of electrical heating rather than laser heating is described. In addition to providing information about the validity of the approach, it is also possible to extract the heat capacity of unknown samples using existing laser calorimetry apparatus. The analysis of the laser calorimetric data is discussed from a more general point of view. An expression for the absorption coefficient is developed which incorporates heat loss corrections in a systematic way. This should find wide applicability for those involved in laser calorimetry as it provides a better way of analyzing data obtained by existing procedures.

4.1.2. Analysis of Calorimetric Data: Heat Loss Corrections

The analysis of adiabatic calorimetric data can be carried out to the following degrees of complexity:

(1) The slope of temperature-time curve is used directly to calculate the absorption coefficient with all heat loss corrections ignored. This can be satisfactory for small temperature rises in a vacuum calorimeter (denoted as "one-slope" method).

(2) The slope of the temperature-time curve is corrected for sample heat losses to calculate the absorption coefficient. However, the sample initially is left in the calorimeter sufficiently long to have achieved a steady state temperature. This is the approach used by most investigators (denoted as "two-slope" method).

(3) The slope of the temperature-time curve is corrected for sample heat losses and the analysis is

sufficiently general so that it need not be assumed that the sample has achieved a steady initial temperature. To the best of our knowledge, this type of analysis has not been employed although it is very convenient when samples of low absorption coefficient are measured with low power lasers (denoted as the "three-slope" method).

These various degrees of approximation are shown schematically in Fig. 1. As mentioned above, most investigators have allowed the sample to come to an initial steady state temperature and then corrected for sample heat losses. This is denoted as a "two-slope" method since the heating and final cooling slopes are employed, although the way in which this correction is introduced depends upon the investigators. Properly employed, this appears to be a perfectly satisfactory way of analyzing the data. However, for the sake of generality, the real situation in which the sample need not be initially at a constant temperature has been analyzed. Since the initial cooling slope, the heating slope, and final cooling slopes are all employed, this is denoted as the "three-slope" method. In practice, since low loss materials are studied with a low power laser, it is often convenient and quicker not to have to wait until the sample reaches a steady state. Because the data acquisition procedures are exactly the same for all situations, it is possible to analyze all adiabatic calorimetric data in this way with only a little extra effort in reading the charts.

In the simple "one-slope" analyses, a sample is irradiated with a laser beam of constant intensity. The absorption coefficient β is related to the slope of the temperature-time curve by the expression

$$mc\left(\frac{dT_2}{dt}\right) = \beta \ell P_t \left(\frac{n^2+1}{2n}\right) \qquad (1)$$

where ℓ = sample length
P_t = transmitted power
m = sample mass
c = heat capacity
n = sample index of refraction
dT_2/dt = slope of temperature-time heating curve

The term $[(2n/(n^2+1)]$ is a correction for multiple reflections deduced independently by Horrigan (1) and Weill (2). In any real situation, some heat losses will occur so that the temperature-time curve will not be a straight line.

These heat losses will be lower in vacuum. However, it is often easier to carry out measurements in air w[illegible] higher losses. In order to correct for these losses [illegible] simple systematic way, the following three-slope anal[illegible] was developed.

In the general case, the sample need not initially be at a constant temperature. As illustrated in Fig. 2, the system can be divided into the following three regions: (1) before laser irradiation; (2) during later irradiation; and (3) after irradiation. The heat balance equations in each of these regions can be given to a first approximation as:

$$mc\left(\frac{dT_1}{dt}\right) + \sigma'\,(T_1^4-T_o^4) + \gamma'(T_1-T_o) = 0 \quad \text{Region I} \quad (2a)$$

$$mc\left(\frac{dT_2}{dt}\right) + \sigma'\,(T_2^4-T_o^4) + \gamma'(T_2-T_o) = \beta\,\ell\,P_t\left(\frac{n^2+1}{2n}\right) \quad \text{Region II} \quad (2b)$$

$$mc\left(\frac{dT_3}{dt}\right) + \sigma'\,(T_3-T_o) + \gamma'(T_3-T_o) = 0 \quad \text{Region III} \quad (2c)$$

Here σ' refers to a radiation loss constant, and γ' involves a constant for conduction and convection losses. The terms, T_1, T_2, and T_3, refer to sample temperatures in the three regions, while T_o refers to the temperature of the surroundings, which is constant throughout the experiment. In all cases, the sample temperature is increased only slightly during laser irradiation so that $T-T_o$ can always be considered small compared to T_o. As a result, the radiation term can be rewritten as:

$$\sigma'(T^4-T_o^4) = \sigma'(T-T_o)(T_1+T_o)(T^2+T_o^2)$$

in which only the term $T-T_o$ changes to any extent during the course of an experiment. Consequently, Eq. (2a), (2b), and (2c) can be simplified to:

$$mc\,\frac{dT_1}{dt} + \sigma(T_1-T_o) = 0 \quad \text{Region I} \quad (3a)$$

$$mc\,\frac{dT_2}{dt} + \sigma(T_2-T_o) = \beta\,\ell\,P_t\left(\frac{n^2+1}{2n}\right) \quad \text{Region II} \quad (3b)$$

$$mc\frac{dT_3}{dt} + \sigma(T_3-T_o) = 0 \qquad \text{Region III} \quad (3c)$$

in which all heat loss terms now involve terms linear in $T-T_o$ and can be lumped together with σ as the coefficient. In regions I and III, Eq. (3a) and (3c) indicate an exponential temperature decrease which is expected and is observed if the sample is at a higher temperature than the surroundings. In region II, the situation is more complicated. In order to evaluate the absorption coefficient β, the heat loss parameter σ and the background temperature T_o are unknown parameters in the expression. By combining Eq. (3a), (3b), and (3c), it is possible to express the absorption coefficient β in terms of measurable quantities. Thus, by subtracting Eq. (3a) from (3c) and rearranging, one obtains

$$\sigma = -mc\left(\frac{T_3'-T_1'}{T_3-T_1}\right) \qquad (4)$$

where $T' = dT/dt$. By subtracting Eq. (3b) from (3a) and substituting the value of σ from Eq. (4), one obtains

$$mc\left[T_2'-T_1'-(T_3'-T_1')\left(\frac{T_2-T_1}{T_3-T_1}\right)\right] = \beta\ell P_t\left(\frac{n^2+1}{2n}\right) \qquad (5)$$

in which the temperature appears as a time derivative (T_1',T_2',T_3') and as temperature differences (T_2-T_1, T_3-T_1), which are easily measurable. That is, use of Eq. (5) is very simple and very general. Three points in each of the three regions of the temperature-time curve are chosen. No special points need be selected except that the regions shortly after the laser is turned on or off should be avoided. The slopes in each of these regions is necessary as well as the temperature differences T_2-T_1 and T_3-T_1, as indicated in Fig. 2.

At NRL, this technique has been adopted as the standard procedure and a program card has been written for the Wang Series 310 Calculator to expedite its use. The approach used is readily adaptable to any programmable calculator or microcomputer. The functional form of Eq. (5) was checked on several samples of typical size and found to hold to a good approximation. As will be discussed in the next section, there may be some inadequacy in the heat loss expressions under some conditions.

The heat balance Eq. (5) is recommended for calculation of absorption coefficients as it encompasses existing

simpler ways of accounting for heat losses in a simple, systematic way. Since it is not assumed that the sample need be at equilibrium initially, this can speed up results.

Finally, it should be noted that this analysis is unable to separate out surface from bulk absorption effects. These still have to be evaluated by measuring the sample as a function of length. In addition, scattering of the radiation can be observed in some samples and this would involve some modification of the formulas derived.

4.1.3. Electrical Simulation and Heat Capacity

One of the problems in laser absorption calorimetry has been the lack of a good standard with which to check out the system. Not only are the absorption coefficients of low loss materials highly variable due to impurities and surface effects, but the uniformity of samples and sample surfaces cannot be guaranteed. Consequently, as a check on the system, simulation of laser absorption heating was attempted by electrical resistance heating. This approach serves several purposes. First of all, by use of a known heat input, it is possible to calculate the specific heat of the sample, a quantity which has been measured in other ways. Agreement between the measurements and the accepted values would strongly imply that the calorimetric aspects of the measurement were satisfactory. It does not imply that all aspects of laser calorimetry are satisfactory, as scattered light corrections are sometimes difficult to account for. Secondly, a way of measuring the specific heat would be of some value for samples where this quantity is not known. The same apparatus as used in laser calorimetry can be employed.

The measurements can be carried out in the following way. One-eighth watt electrical resistors are placed inside holes drilled in the sample. These resistors are about 1.5 mm diameter and 4 mm long, which is comparable to the intercepted volume of the laser beam. To insure good thermal contact, they are cemented with a small amount of epoxy adhesive. Fine copper leads are attached to limit the thermal conductivity. A sample with a resistor in the interior is shown in Fig. 3. Heat is supplied electrically to simulate laser beam absorption at about the same power level. The current and resistance are measured with a calibrated digital meter. The temperature of the sample is measured in the same way as in laser absorption calorimetry and the temperature-time curve is analyzed using a modification of Eq. (5),

$$i^2R/mc = T_2' - T_1' - (T_3'-T_1)[(T_2-T_1)/(T_3-T_1)]. \quad (6)$$

This can be solved readily for the heat capacity c in terms of known parameters.

The heat capacity of KCl, NaCl, and LiF, for at least two samples of each material, has been calculated and the results are shown in Table 1. The deduced values seem to be uniformly about 5-15% higher than the accepted values. While this agreement can be considered satisfactory, it is somewhat higher than can be accounted for from any specific reason. It is felt that the source of this error could be established if desired, but this has not been attempted because it was not felt to be a serious problem.

These results suggest that the heat capacity of materials can be obtained to within about 10% accuracy by use of a laser calorimetry system. The deduced specific heat would be apt to be on the high side.

In addition to system checkout and the determination of unknown heat capacity, the electrical simulation approach may be useful for another purpose as well; namely, when large diameter windows become available, there may be some question about the validity of the approach when the sample is heated by a small laser beam on one side and measured at the edge with a thermocouple. Due to a finite thermal conductivity, the sample may not heat up uniformly and so heat-balance expressions such as Eq. 5, which assume uniform temperature distributions, may not be completely valid. Consequently, it may be helpful to check out such geometries using electrical simulation. Such measurements were carried out with smaller sample blocks in which thermocouples have been placed in different parts of the sample. Differences of the order of 10% were noted, depending upon thermocouple placement. This may very well be due to a non-uniform temperature distribution which is not a problem for present sample sizes and accuracies. However, it could be a problem if higher accuracies or large samples would be examined.

Finally, the question of assuring good thermal contact of the temperature sensor can be raised. At NRL, the policy was to place the thermocouple inside a hole drilled in the sample. Thermal contact is made with Dow Corning 340 heat sink compound.

1. F. A. Horrigan and T. F. Deutsch, "Research in Optical Materials and Structures for High-Power Lasers," QTR No. 2, Contract DAAH01-72-C-0194, ARPA Order No. 1180, April 1972.

2. R. Weill, "Calculation of Small Optical Absorption Coefficients from Calorimetric Experimental Data," J. Appl. Phys. 41, 3012 (1970).

3. K. H. Rosette, C. F. Swinehart, E. F. Shrader, D. H. Hammond, G. Kramer, P. H. Moss, H. Packer, S. Stotlar, M. R. Farukhi, F. Pecjak and P. Nemeth, "Chemically Strengthened Polycrystalline Potassium Chloride," QPR No. 1, Contract No. F33615-72-C-2160 (AFML), Harshaw Chemical Co. (1972).

Table 1

HEAT CAPACITY DETERMINATION

Material	Mass gr	c_p Observed J/gram-°K		c_p Accepted J/gr-°K	Deviation %
KCl	3.29	0.779 0.796 0.806	0.793	0.68	+ 17
KCl	6.14	0.797 0.786 0.835	0.805	0.68	+ 18
KCl	20.34	0.774 0.725 0.743	0.747	0.68	+ 10
NaCl	3.85	0.950 0.993	0.971	0.85	+ 14
NaCl	6.00	0.872 0.913 0.894	0.893	0.85	+ 5
LiF	3.70	1.697 1.702 1.849	1.75	1.56	+ 13
LiF	7.94	1.707 1.687 1.674 1.739 1.678	1.697	1.56	+ 9

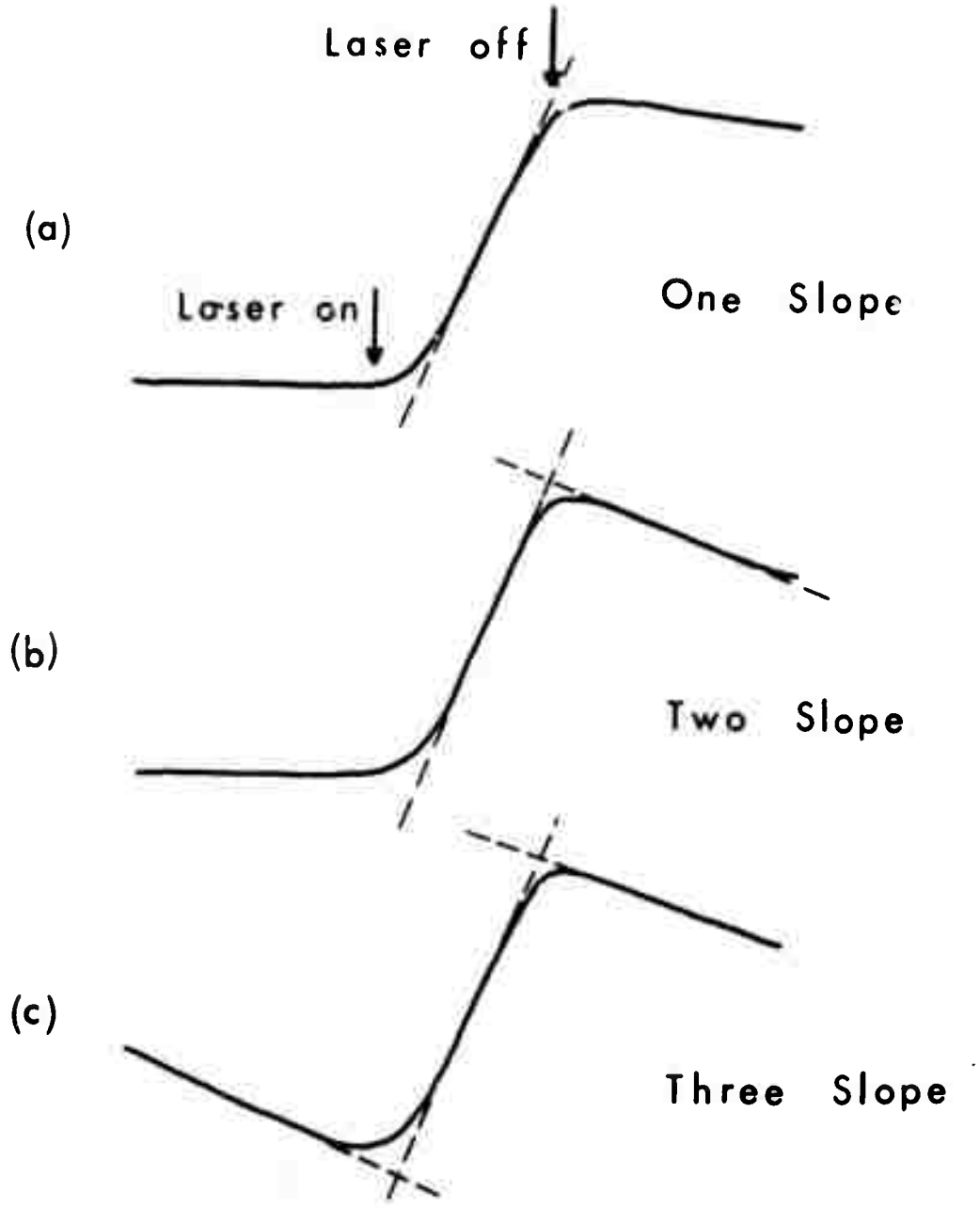

Fig. 1. Typical temperature-time curves for laser calorimetry. Depending on the temperature rise and conditions (air or vacuum). Curves (a), (b), and (c) will be observed with (c) being the most general case.

(a) Typical temperature-time curve for a case where one-slope analysis is valid.
(b) Typical temperature-time curve for case where two-slope analysis is valid.
(c) Typical temperature-time curve for case where three-slope analysis is valid.

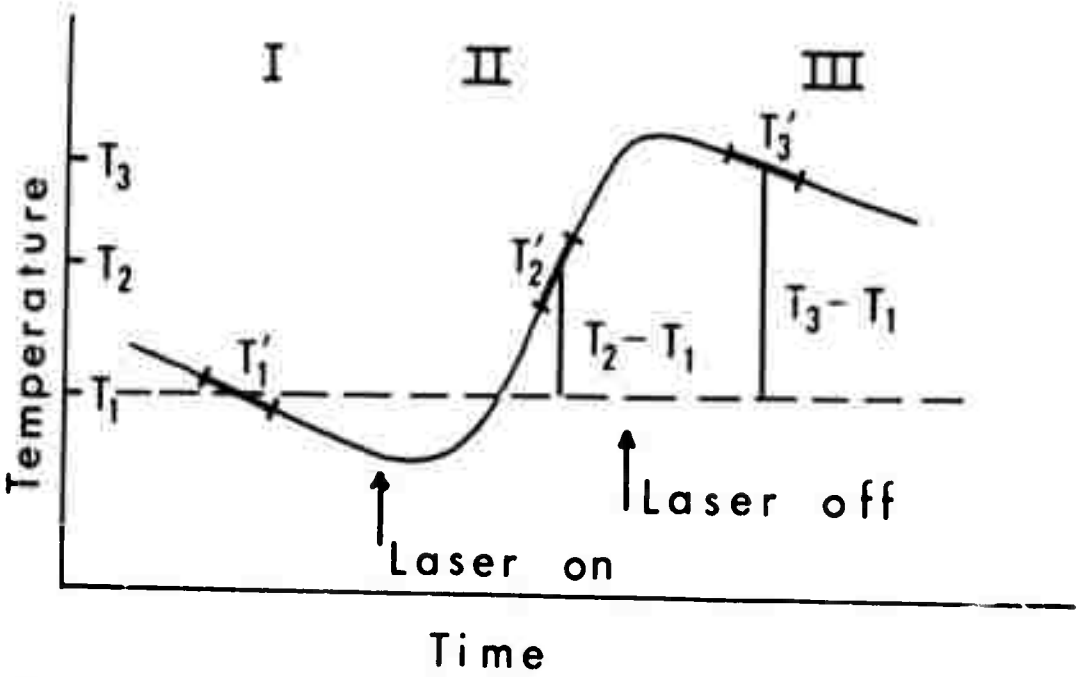

Fig. 2. Selection of points on temperature-time curve. The slope T_2' is positive and T_1' and T_2' are usually negative. The absolute temperature T_1 need not be known.

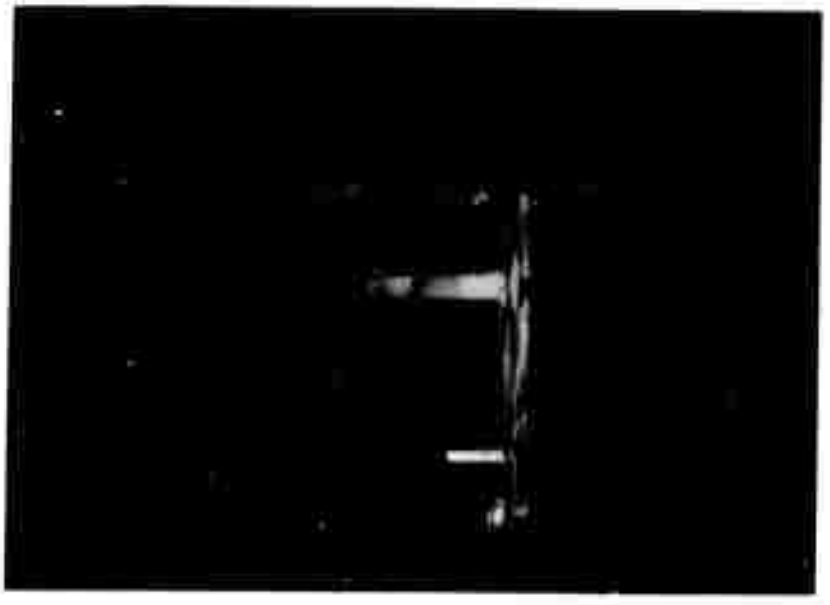

Fig. 3. KCl crystal with one-eighth watt carbon resistor embedded in it.

4.2. Absorption Measurements, M. Hass, F. W. Patten, J. A. Harrington, J. W. Davisson

Optical absorption measurements on some of the materials described elsewhere in this report are summarized and discussed in this section. These measurements were obtained using the techniques described in the previous section. The following samples were studied: (1) thallium chloride; (2) Sr-doped KCl crystal; (3) Oak Ridge high purity KCl; (4) Hughes high purity KCl; and NRL press forged material from Hughes KCl.

4.2.1. Single Crystals

(1) Thallium chloride crystals

The thallium chloride crystal, discussed in Section 2.1, was used for absorption measurements. The fractional power absorbed, $\beta\ell$, was 0.005 for both 1 and 2 cm thickness. This suggests that the surface absorption is the dominant source of absorption, just as was the case for the first specimens of KCl that were studied. In addition, the temperature-time curve for the calorimetry apparatus indicated that a large amount of radiation was scattered. As noted in Section 2.1, it is uncertain whether TlCl merits development.

(2) 0.1 m/o $SrCl_2$-KCl crystal (see Section 2.1)

The fraction absorption in this crystal was 0.01 for a one-centimeter thickness, which is comparable to poor quality KCl crystals. As mentioned in Section 2.1, the OH^- content may be high in this alloyed crystal, which could account for the higher absorption value. In support of this, Rosette et al (3) have shown that small (50 up to 1000-2000 ppm molar) additions of $SrCl_2$ have negligible effect on the absorption of KCl crystals. Thus, the effects of divalent dopants in the range of 100-1000 ppm molar on the absorption of much purer KCl crystals will be studied in conjunction with forging studies.

(3) Oak Ridge high purity KCl crystal (obtained from W. Sibley, Oklahoma State University)

The results in Table 1 are incomplete as the available sample limited measurements to two thicknesses. However, it is evident from that data that the value of β appears to be 0.001 cm^{-1} or less and that surface absorption is very low. This could be confirmed by studying additional thicknesses. The absorption in the above chemically polished samples was essentially uniform. Work of this nature on Cornell crystals will be carried out in the next quarter.

(4) Hughes KCl crystal

The two values for $\beta\ell$ in Table 1 are for two different chemical polishings of this crystal. These results indicate that although the maximum absorption coefficient β ranges between 0.00046 cm^{-1} and 0.00079 cm^{-1}, the chemical polishing procedure is subject to some variations. A variability has also been noted in absorption coefficient as a function of position in some chemically polished single crystal specimens; that is, if the specimen is left to drain in a vertical position, then the absorption at the bottom is higher than at the top. By altering the polishing procedure, this can be minimized.

4.2.2. Press forged KCl (Hughes starting crystal)

The results for this material showed a large variation with location of the beam. Fractional power absorbed ($\beta\ell$) ranged from a low of 0.002 to about 0.01 for samples of both 1 and 2 cm nominal thickness, as shown in Fig. 1. Here the higher values might well be attributed to local regions of high absorption in either the surface or bulk. The chemical polishing procedures for press forged materials have not been developed as well as for single crystals. In the case of cleaved crystal materials, corresponding variations as a function of position have also been observed. In such cleaved crystals, the lowest value of the absorption appeared to be closest to that for a good chemical polished surface. If similar arguments are employed for these press forged materials, this would suggest an absorption coefficient of around 0.002 cm^{-1} as a tentative value. The actual value might be as low as that of the starting material which was in the range of 0.0005-0.0008 cm^{-1}.

If the above reasoning is accepted, then the following significant point would be implied: namely, previous results at NRL and other laboratories using Harshaw KCl starting material having an absorption coefficient of 0.002 cm^{-1} have resulted in press forged samples with absorption coefficients of around 0.01 cm^{-1}. An important question is whether use of starting material having a much lower absorption coefficient would result in a corresponding decrease in the press forged results. These results suggest that it does, although the improvement in the press forged results might be due in part to the improved chemical polishing technique employed.

In spite of the lower value of the absorption coefficient, which seems to be suggested by this new data, it is disturbing to note the large variation as a function of position of the beam. This behavior is probably characteristic of all of the press forged materials produced and not unique to this specimen or to this Laboratory. Two questions arise which will require further investigation: (1) Is the absorption associated with the surface, bulk, or both; and (2) Can the variation be reduced by a large amount?

In response to the first question, it is believed that at least part of the variation is due to surface effects which have been the bane of all investigators in this area. In chemically polishing press forged material, the length of time in which the sample is immersed alters the final appearance. If the sample is immersed for a long time, then grain structure becomes apparent. The optimum conditions for a chemical polish on forged materials has not yet been established. It would involve work along the lines indicated for the single crystals in which the absorption is measured as the polishing conditions are varied.

In considering the second question, it is noted that the polycrystalline nature of the press forged material, and hence its surface, may be similar to the surface layers of an imperfectly cleaved crystal. In such crystals, the absorption is markedly dependent on position of the probe laser beam. Consequently, it may not be surprising to observe additional absorption for the forged material. It remains to be seen whether processing, such as annealing which tends to smooth out crystalline discontinuities, will result in lower loss. Voids and impurities such as OH^- or O_2 might enter during forging and become locally segregated, e.g., as grain boundaries, to cause variable absorption. Such impurities might become more homogeneously distributed by annealing. In addition, remelting of a press forged material to form a single crystal again might indicate something if the absorption coefficient of the starting and final single crystal were different.

The main point is that the absorption of forged materials presents a complex problem. There are apt to be large local variations which are now beginning to be recognized by using higher quality crystals. When these variations are reduced to a manageable level, then measurements as a function of length can be employed to separate out surface and bulk absorption in the usual way. Even more importantly, these large variations will have to be

reduced before press forged materials can be used for operational laser windows. More recent absorption measurements where the press forged sample was carefully repolished (mechanically and then chemically) resulted in reducing the data scatter and in achieving absorption values very comparable to the parent Hughes single crystal. These results indicate that further refinement of the polishing techniques could lead to further reduction in absorption and that the variable results are closely associated with surface finish.

4.2.3. Future Studies

Surface versus bulk absorption in KCl crystals, particularly for high purity KCl crystals with various surface finishes will be determined. Similar studies will be made of press forged materials, especially the Hughes high purity crystal forgings. In addition, the effects of annealing on the point-to-point variation of absorption in the forgings will be examined, together with the effects of forging procedure on absorption (2.2.4.). Studies on the temperature dependence of the absorption of single crystals will continue and be compared with theoretical absorption dependence to determine if absorption is extrinsic or intrinsic limited. Additional work will deal with the effects of radiation hardening and divalent doping on the absorption of KCl crystals.

Table 1

ABSORPTION MEASUREMENTS

Material	Fractional Absorption $\beta\ell$	Length ℓ, cm
TlCl crystal	0.005	1
	0.005	2
ORNL HP[1] KCl crystal[2]	0.0007	0.41
	0.0011	0.76
Hughes HP[1] KCl crystal	0.0011	2.4
	0.0019	

[1] HP: high purity

[2] Oak Ridge National Laboratory crystal obtained from W. Sibley, Oklahoma State University.

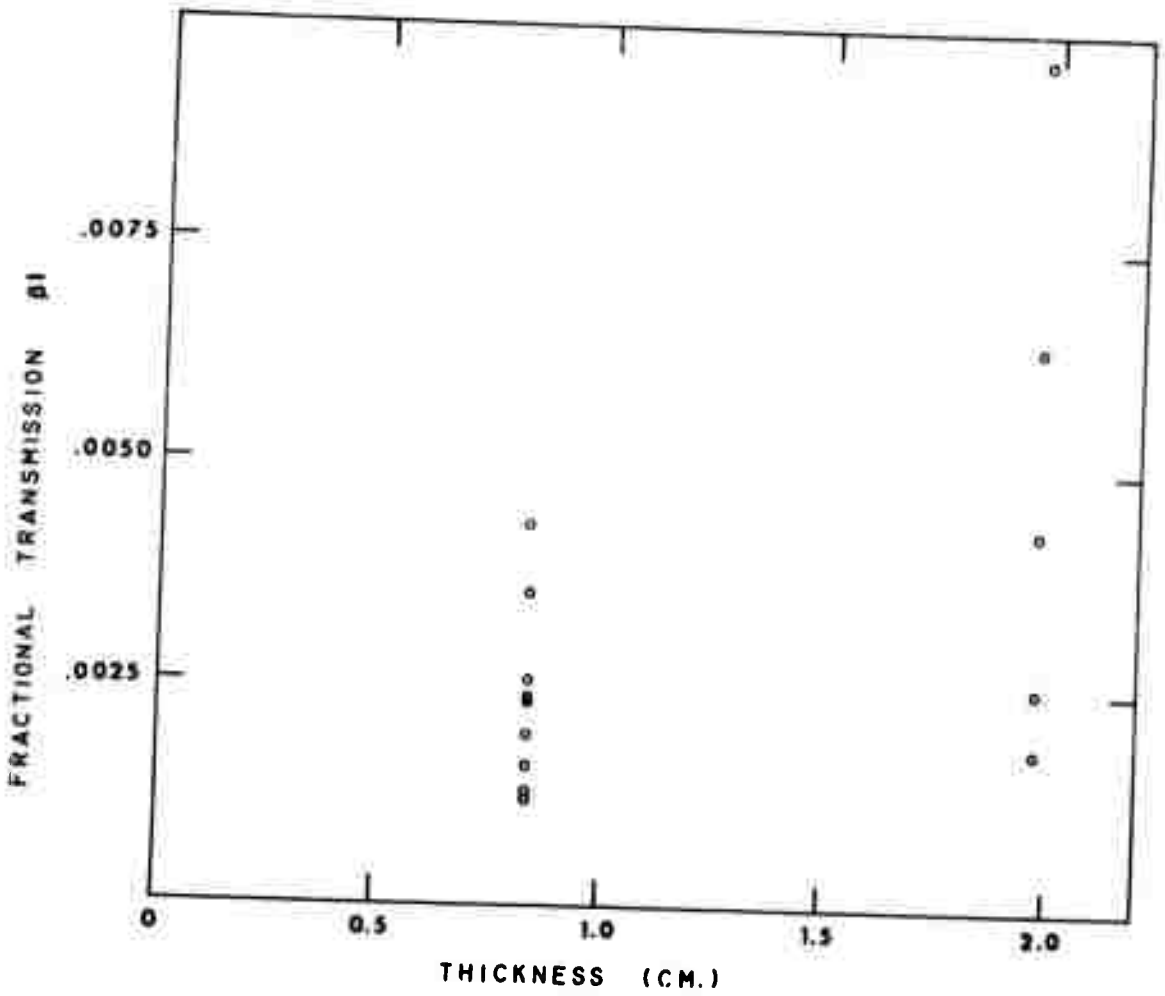

Fig. 1. Fractional transmission β for forged KCl (Hughes starting material). The points indicated are different locations on the same sample for two sample lengths. The surfaces were chemically polished. Because of the variability in transmission, it is not appropriate to extract the absorption coefficient, β. However, it appears that a value of β of 0.0025 cm^{-1} or less is achievable. Note: Recent results after repolishing show β values comparable to the starting Hughes crystal and variability is substantially reduced.

5.0. THEORETICAL ANALYSIS

Multiphonon Absorption by Ionic Crystals: Temperature Dependence

Herbert B. Rosenstock

Abstract

In this work, we consider the part of the temperature dependence of the multiphonon absorption in the IR that is not dependent on the mechanism from which the absorption arises. Several phonons must act together to provide absorption at high frequencies; the availability of each phonon alone provides a temperature dependence that is the same whatever the mechanism for coupling them together may be. These availability factors must then be summed over the existing frequency distribution in a particular crystal, subject to the condition that the sum of frequencies equal that of the incoming light. Numerical results are given for KCl at 10.6 microns. We find the temperature dependence to be different depending on whether the incoming photon couples to a lattice or an impurity phonon of higher frequency. This suggests experiments that could reveal whether the residual absorption found in nominally "pure" crystals is in fact intrinsic or due to unknown impurities.

5.1. Formal Derivation

Consider the process of n phonons of frequency ω_i absorbing a photon of frequency

$$\omega = \sum_i^n \omega_i \quad . \tag{1}$$

Call theprobability for that process at temperature T

$$p_n = p_n(\omega_1, \omega_2, \ldots \omega_n, T). \tag{2}$$

(We ignore difference bands for the moment; for these, some of the ω_i would enter (1) with a negative sign). The probability of absorption of a photon of frequency ω is then

$$P_n(\omega, T) = \int \cdots \int d\omega_1 \ldots d\omega_n \, p_n \, \delta(\omega - \sum_i^n \omega_i), \tag{3}$$

because each phonon involved can have any frequency, subject only to the restriction (indicated by the delta function) that the sum of all phonon frequencies be ω.

A special restriction arises from the fact that one of the modes must couple directly to the electromagnetic field, and only certain modes are capable of doing that, since others lack a dipole moment. For the pure lattice, this is the "dispersion oscillator" or "restrahl" mode; for an impure one, a "local" impurity mode can also serve. (We ignore the possibility that in an impure lattice the slightly perturbed lattice modes may also have a nonvanishing dipole moment.) Let us call this mode - either the restrahl or the local mode - a "coupling" mode, denoted by subscript c. We must then introduce into (3) a factor $\delta(\omega_n - \omega_c)$ and get

$$P_n(\omega,T) = \int \cdots \int d\omega_1 \cdots d\omega_{n-1}\, p_n\, \delta\Big(\omega - \omega_c - \sum_1^{n-1}\omega_i\Big). \quad (4)$$

Let us now consider the form of p_n. It consists of two parts, the temperature dependent part that comes from the probability of finding each oscillator in a given excited state, and the probability of finding an oscillator of that fundamental frequency in the lattice. The first part is given by

$$\prod_{i=1}^{n}(1+F_i) - \prod_{i=1}^{n} F_i \quad (5)$$

with

$$F_i \equiv F(\omega_i) = \left[e^{\hbar\omega_i/kT} - 1\right]^{-1}. \quad (6)$$

It is important to realize the general validity of this expression. It results simply from summing over all possible states that the oscillator can be in, and is quite independent of the mechanism by which the oscillators are coupled. The result is therefore valid for any such mechanism, be it an anharmonic potential, a high order multipole or dipole moment, etc. (See appendix II for a brief derivation).

The second is the "density of states" or frequency distribution $g(\omega)$, a rather complicated function that is not really known with certainty for many crystals and that we shall crudely approximate by Debye's method.

Before we proceed, it is convenient to introduce dimensionless variables. We let

$$E_i = \hbar\omega_i / \hbar\omega_R$$
$$E_c = \hbar\omega_c / \hbar\omega_R$$
$$E = \hbar\omega / \hbar\omega_R \qquad (7)$$
$$\tau = kT / \hbar\omega_R$$

where ω_R is the restrahl frequency, which we assume to be the highest frequency in the lattice band, so that each dimensionless phonon energy runs from 0 to 1. E_c is unity if the coupling is via the restrahl oscillator, different from unity (and presumably larger) if it is due to a local oscillator.

In terms of the dimensionless variables, (6) is

$$\bar{F}_i \equiv F(\omega_i) = \left[e^{E_i/\tau} - 1 \right]^{-1} \qquad (8)$$

and the Debye approximation to the frequency distribution

$$g(E_i) = \begin{cases} 3E_i^2 & 0 < E_i < 1 \\ 0 & \text{otherwise.} \end{cases} \qquad (9)$$

The factor 3 provides proper normalization, but will be omitted from now on (as are many other constant terms multiplying P_n). (3) thus becomes

$$P_n(E,\tau) = \int \cdots \int \left[(1+F_c) \prod_1^{n-1} (1+F_i) - F_c \prod_1^{n-1} F_i \right] \delta\left(E - E_c - \sum_1^{n-1} E_i\right) \cdot \qquad (10)$$
$$\cdot \prod_1^{n-1} E_i^2 \, dE_i$$

5.2. Evaluation

For n = 1 and 2, the evaluation of (10) is nearly trivial. When n = 1, there are no terms at all in the sum, and no integrals; we see that (10) becomes

$$P_1(E,\tau) = \delta(E - E_c) , \tag{11}$$

a simple line spectrum independent of temperature - the well-known result for one-phonon absorption.

When n = 2, (10) becomes

$$P_2 = \int_0^1 E_1^2\, dE_1 \left[(1+F_c)(1+F_1) - F_c F_1\right] \delta(E - E_c - E_1) \tag{12}$$

$$= \begin{cases} E_D^2 \left(1 + F_c + F_D\right) & 0 < E_D < 1 \\ 0 & \text{otherwise} \end{cases}$$

where we have introduced

$$E_D = E - E_c , \qquad F_D = F(E_D) . \tag{13}$$

For n = 3 or greater, it is best to use the representation (A3) for the Dirac Delta function; otherwise the various conditions imposed by the delta function and the limits on the multiple integrals become hard to keep track of. After interchanging the order of the integrations, (10) becomes

$$P_n(E,\tau) = (2\pi i)^{-1} \int_{\gamma - i\infty}^{\gamma + i\infty} ds\, e^{E_D s} \left[\left(1+F_c\right) J^{n-1}(s,\tau) - F_c I^{n-1}(s,\tau)\right] , \tag{14}$$

for the integrals over each of the E_i are now the same:

$$J(s,\tau) = \int_0^1 dx\, x^2 e^{-sx} \left[1 + F(x)\right] \tag{15}$$

and

$$I(s,\tau) = \int_0^1 dx\, x^2 e^{-sx} F(x) \tag{16}$$

with

$$F(x) = \left[e^{x/\tau} - 1\right]^{-1} . \tag{17}$$

The first part of J is elementary, and the second part is identical with I; we find

$$J(s,\tau) = I(s,\tau) + K(s) \tag{18}$$

where

$$K(s) = 2 s^{-3}\left[1 - e^{-s} f(s)\right] \tag{19}$$

$$f(s) = 1 + s + \tfrac{1}{2} s^2 \tag{20}$$

but were not able to integrate I in closed form for all τ, and must therefore resort to separate expansions for high and low T.

Large τ ($\tau > 1$, $kT > \hbar\omega_R$).

We expand (17) as

$$F(x) = \left[1 + (x/\tau) + (x/\tau)^2/2 \cdots - 1\right]^{-1}$$
$$\cong (\tau/x)\left[1 - x/2\tau + \cdots\right]$$
$$= \tau/x - \tfrac{1}{2} ;$$

I then becomes

$$I(s,\tau) = \tau L(s) - \tfrac{1}{2} K(s) \tag{21}$$

with

$$L(s) = s^{-2}\left[1 - e^{-s} g(s)\right] , \tag{22}$$

$$g(s) = 1 + s , \tag{23}$$

and, on account of (18),

$$J(s) = \tau L(s) + \tfrac{1}{2} K(s) . \tag{24}$$

To proceed further, we need to specify the order of the process. We let, most simply for a first try, n = 3 in (14) - a three phonon process (one "coupling" and two "lattice" phonons). The bracket in (14) then becomes

$$\left[(1+F_c) J^2 - F_c I^2\right] = \tau^2 L^2 + 2(2F_c + 1)\tau L K + \tfrac{1}{4} K^2 \tag{25}$$

with additional terms, in inverse powers of τ, omitted because the expansion of F was truncated.

After some algebra and integration with help of (A3), (14) becomes

$$P_{13}(E,\tau) = \tau^2 M_2(E_D) + 2(2F_c+1)\tau M_1(E_D) + M_0(E_D) \tag{26}$$

where

$$M_2(x) = S_3(x) - 2\left[S_3(x-1) + S_2(x-1)\right] + \left[S_3(x-2) + 2S_2(x-2) + S_1(x-2)\right]$$

$$M_1(x) = S_4(x) - \left[2S_4(x-1) + 2S_3(x-1) + \tfrac{1}{2}S_2(x-1)\right] + \left[S_4(x-2) + 2S_3(x-2) + \tfrac{3}{2}S_2(x-2) + \tfrac{1}{2}S_1(x-2)\right]$$

$$M_0(x) = S_5(x) - \left[2S_5(x-1) + 2S_4(x-1) + S_3(x-1)\right] + \left[S_5(x-2) + 2S_4(x-2) + 2S_3(x-2) + S_2(x-2) + \tfrac{1}{4}S_1(x-2)\right] \quad (27)$$

with the $S_j(x)$ defined by (A1), with $E_D = E - E_C$ as before.

For physical reasons, $P_3(x)$ must be 0 for $x > 2$ (for the absorbed photon energy E greater than $E_C + 2$, the sum of the maximum energies of the three phonons) and this can be verified for each of the three M's in (27), though perhaps it is not obvious on sight.

For our practical application, we shall need P_5 and P_7. The process is quite the same, beginning with putting $n = 5$ instead of (3) into (14), but the algebra is a little more involved. We find that (26) is replaced by

$$P_5(E,\tau) = \tau^4 N_4(E_D) + 2\left(2F_1 + 1\right)\tau^3 N_3(E_D) + \tfrac{3}{2}\tau^2 N_2(E_D) \quad (28)$$

with terms $O(\tau)$ omitted, and the N's are given by

$$\left.\begin{matrix} N_4(x) \\ N_3(x) \\ N_2(x) \end{matrix}\right\} = (2\pi i)^{-1}\int_{\gamma-i\infty}^{\gamma+i\infty} ds\, e^{xs} \left\{\begin{matrix} L^4 \\ L^3K \\ L^2K^2 \end{matrix}\right. \quad (29)$$

and evaluated as

$$N_j(x) = \sum_{l=0}^{j} (-)^l \binom{j}{l} Y_l^{(j)}(x) \qquad (j = 4, 3, 2)$$

$$Y_l^{(4)}(x) = \sum_{k=0}^{l} \binom{l}{k} S_{7-k}(x-l)$$

$$Y_l^{(3)}(x) = 2 \sum_{k=0}^{l} \binom{l}{k} \left\{ S_{8-k}(x-l) - T_{8-k}(x-l-1) \right\} \qquad (30)$$

$$Y_l^{(2)}(x) = 4 \sum_{k=0}^{l} \binom{l}{k} \left\{ S_{9-k}(x-l) - T_{9-k}(x-l-1) + U_{9-k}(x-l-2) \right\}$$

$$T_{h-k}(x) = S_{h-k}(x) + S_{h-k-1}(x) + \frac{1}{2} S_{h-k-2}(x)$$

$$U_{h-k} = S_{h-k}(x) + 2 S_{h-k-1}(x) + 2 S_{h-k-2}(x) + S_{h-k-3}(x) + \frac{1}{4} S_{h-k-4}(x)$$

Again each N vanishes identically for x > 4, as it must for physical reasons (though the reader will require some minutes of algebra to verify this).

In the very same way, we obtain for n = 7

$$P_7(E,\tau) = \tau^6 R_6(E_D) + 6\tau^5 (2F_C + 1) R_5(E_D) + 15\tau^4 R_4(E_D) \qquad (31)$$

where

$$R_j(x) = \sum_{l=0}^{j} (-)^l \binom{j}{l} Z_l^{(j)}(x) \qquad (j = 6, 5, 4)$$

with

$$Z_l^{(6)}(x) = \sum_{k=0}^{l} \binom{l}{k} S_{11-k}(x-l)$$

$$Z_l^{(5)}(x) = \sum_{k=0}^{l} \binom{l}{k} \left\{ S_{12-k}(x-l) - T_{12-k}(x-l-1) \right\}$$

$$Z_l^{(4)}(x) = \sum_{k=0}^{l} \binom{l}{k} \left\{ S_{13-k}(x-l) - 2 T_{13-k}(x-l-1) + U_{13-k}(x-l-2) \right\}$$

and T and U given by (30).

Small τ ($e^{1/\tau} \gg 1$, $kT \lesssim \hbar\omega_R$).

When τ is small, we can expand at F as

$$F(x) = \left(e^{x/\tau} - 1\right)^{-1} = e^{-x/\tau}\left(1 - e^{-x/\tau}\right) = \sum_{j=1}^{\infty} e^{-jx/\tau} \tag{32}$$

so that I of (16) becomes

$$I(s,\tau) = \sum_{j=1}^{\infty} \int_0^1 dx\, x^2 e^{-[s+(j/\tau)]x}$$

In the notation (19) this is

$$I(s,\tau) = \sum_{j=1}^{\infty} K(s+j\beta) \tag{33}$$

and by (18)

$$J(s,\tau) = \sum_{j=0}^{\infty} K(s+j\beta) \tag{34}$$

where we have written

$$\beta = 1/\tau . \tag{35}$$

For the evaluation of P_n, this is to be put in (14), where we now need $[(1+F_c)J^{n-1} - F_c I^{n-1}]$. As β is large, we shall retain negative powers of β, but neglect all terms that contain $-\beta$ in the exponent. With this criterion, we immediately neglect F_c in the bracket in (14) which becomes simply J^{n-1} and (14) itself becomes

$$P_n(E,\tau) = (2\pi i)^{-1} \int_{\gamma-i\infty}^{\gamma+i\infty} ds\, e^{E_0 s} \left[\sum_{j=0}^{\infty} K(s+j\beta)\right]^{n-1} . \tag{36}$$

We shall carry out the calculation for n = 3 only. From (36) we have

$$P_3(E,\tau) = \sum_{j=0}^{\infty} R_{jj} + 2\sum\sum_{\ell>j\geq 0} R_{j\ell} \tag{37}$$

with

$$R_{j\ell} = (2\pi i)^{-1} \int_{\gamma-i\infty}^{\gamma+i\infty} ds\, e^{E_0 s} K(s+j\beta) K(s+\ell\beta) \tag{38}$$

or, using (20)

$$\frac{1}{4}R_{je} = (2\pi i)^{-1}\int ds\, e^{E_D s}(s+j\beta)^{-3}(s+\ell\beta)^{-3}\left[1-e^{-(s+j\beta)}f(s+j\beta)\right]\cdot \left[1-e^{-(s+\ell\beta)}f(s+\ell\beta)\right]$$

First, consider the case $j=\ell=0$. Then

$$\frac{1}{4}R_{00} = (2\pi i)^{-1}\int ds\, e^{E_D s}\, s^{-6}\,(1-f(s)e^{-s})^2 \qquad (40)$$
$$= M_0(E_D),$$

a quantity already evaluated in (25), (26). Next consider $j=\ell\neq 0$. We can then neglect all f(s) on account of the $e^{-j\beta}$ factor, and are left with

$$\frac{1}{4}R_{jj} = (2\pi i)^{-1}\int_{\gamma-i\infty}^{\gamma+i\infty} ds\, e^{E_D s}(s+j\beta)^{-6}, \qquad (j\neq 0). \qquad (41)$$

Letting $u = s+j\beta$, we have

$$\frac{1}{4}R_{jj} = (2\pi i)^{-1}e^{-j\beta}(2\pi i)^{-1}\int_{\gamma+j\beta-i\infty}^{\gamma+j\beta+i\infty} du\; e^{E_D u}\, u^{-6}$$

The integral can be evaluated in the usual way, but the entire term is negligible on account of the $e^{-j\beta}$ factor.

Now for $j\neq\ell$. If neither j nor ℓ are 0, we can, as above, neglect the f term, being left with

$$\frac{1}{4}R_{j\ell} = (2\pi i)^{-1}\int ds\, e^{E_D s}\,(s+j\beta)^{-3}(s+\ell\beta)^{-3} \qquad (42)$$

and to evaluate this we transform $u = s+j\beta$ to find the values at the pole $-j\beta$, and transform $v = s+\ell\beta$ to find the value at the pole $-\ell\beta$. A factor $e^{-j\beta}$ or $e^{-\ell\beta}$ appears in either case, making these terms negligible. Finally we need the case $j\neq\ell$, but one of them equal 0. Then

$$\frac{1}{4}R_{\ell 0} = (2\pi i)^{-1}\int ds\, e^{E_D s}\, s^{-3}(s+\ell\beta)^{-3}(1-f(s)e^{-s}) \qquad (43)$$

(the $f(s+\ell\beta)$ term having been neglected on account of the exponential that multiplies it.) Poles are located at 0 and $-\ell\beta$, but the latter are, by the transormation $u = s+\ell\beta$, found to contribute negligible

terms of order $e^{-\ell\beta}$, and the former are the only ones that need considering. Let us separate the two terms,

$$\tfrac{1}{4} R_{\ell 0} = A_\ell(E_0) - B_\ell(E_0) \qquad (44)$$

with
$$A_\ell(E_0) = (2\pi i)^{-1} \int ds\, e^{E_0 s}\, s^{-3}(s+\ell\beta)^{-3},$$
$$B_\ell(E_0) = (2\pi i)^{-1} \int ds\, e^{E_0 s}\, s^{-3}(s+\ell\beta)^{-3} f(s).$$

A is zero if $E_D < 0$ (because the contour can be closed to the right, enclosing no poles); for $E_D > 0$, the residue at s=0 can be found by expanding:
$$A_\ell(x) = (2\pi i)^{-1} \int ds\, s^{-3} (\ell\beta)^{-3} \sum_{m=0}^{\infty} \binom{-3}{m} (s/\ell\beta)^m \sum_{k=0}^{\infty} (xs)^k/k!$$
$$= (\ell\beta)^{-3} \sum_{m=0} \binom{-3}{m} (\ell\beta)^{-m} \sum_{k=0} (x^k/k!)(2\pi i)^{-1} \int ds\, s^{\ell+k-3}$$

The integral is $2\pi i$ when $\ell+k-3$ is -1, and zero otherwise, and so
$$A_\ell(x) = (\ell\beta)^{-3} S_2(x) - 3(\ell\beta)^{-4} S_1(x) + 6(\ell\beta)^{-5} S_0(x).$$

Similarly,
$$B_\ell(x) = (2\pi i)^{-1} \int ds\, e^{(x-1)s} \left[s^{-3} + s^{-2} + \tfrac{1}{2} s^{-1}\right] (s+\ell\beta)^{-3}$$

becomes
$$B_\ell(x) = (\ell\beta)^{-3} \left\{ \begin{array}{l} \left[S_2(x-1) + S_1(x-1) + \tfrac{1}{2} S_0(x-1) \right] \\ -3(\ell\beta) \left[S_1(x-1) + S_0(x-1) \right] \\ + 6(\ell\beta)^2 S_0(x-1) \end{array} \right\}$$

Let us summarize:

$$\frac{1}{4} R_{jl} = \begin{cases} M_0(E_D) & j = l = 0 \\ A_l - B_l & j = 0,\ l > 0 \\ A_j - B_j & j > 0,\ l = 0 \\ 0 & j > 0,\ l > 0. \end{cases}$$

Thus, (37) becomes

$$\frac{1}{4} P_3(E, \tau) = M_0(E_D) + 2 \sum_{l=1}^{\infty} [A_l E_3(l) - B_l(E_D)]$$

$$= M_0(E_D) + 2\zeta_3 \tau^3 M_3(E_D) - 6 \zeta_4 \tau^4 M_4(E_D) + 12 \zeta_5 \tau^5 M_5(E_D) \quad (45)$$

where

$$\zeta_3 = \sum_1^{\infty} l^{-3} = 1.20205$$
$$\zeta_4 = \sum_1^{\infty} l^{-4} = 1.08232$$
$$\zeta_5 = \sum_1^{\infty} l^{-5} = 1.03693 \quad (46)$$
$$M_3(x) = S_2(x) - [S_2(x-1) + S_1(x-1) + \tfrac{1}{3} S_0(x-1)]$$
$$M_4(x) = S_1(x) - [S_1(x-1) + S_0(x-1)].$$
$$M_5(x) = S_0(x) - S_0(x-1).$$

and $M_0(x)$ given by (27). It is interesting to note that this vanishes for $E_D > 1$, not just for $E_D > 2$ as did the results of the high temperature expansion, Eq. (26). The absorption in the energy region $1 < E_D < 2$ is evidently exponentially small, such terms having been neglected in this section.

5.3. Numerical Results

Table 1 below applies to KCl. The numbers in the last column have been scaled according to equation (7).

Table 1

Temperature (°K)	wavelength (microns)	energy (ev.)	E or τ (dimensionless)	(comment)
215	70	.018	1.00	KCl restrahl
300			1.39	Room temperature
400			1.85	
600			2.78	
	20	.062	3.44	U-center
	17.5		4.00	
	10.6		6.6	CO_2 laser

We are interested in the T-dependence of the absorption at wavelength 10.6 microns which, according to Table 1, corresponds to E=6.6. Coupling via the restrahl mode (E_c=1) will give absorption by 7-, 8-, 9-,... phonon process -- no fewer, because 6 phonons, each of energy 1, can absorb a photon of energy 6 at most, but not 6.6. Of these, the 7-phonon process will be the most probable. Similarly, coupling via the U-center mode (E_c=3.44) will give absorption by 5-, 6-, 7-,... phonon processes -- no fewer, because 4 phonons, three of energy 1 and one of energy 3.44, can absorb a photon of energy 6.44 at most, but not 6.6. Of these, the 5-phonon process will be the most probable.

We therefore plot on Fig. 1, the expressions $P_5(6.6, \tau)$ and $P_7(6.6, \tau)$, the former for E_c=3.66, the latter for E_c=1. Only the high-temperature expansion of Section II has been used, and one might thereby question the validity of the figure close to $\tau = 1$. As a check, we have therefore computed an analogous quantity, $P_3(2,1)$ for E_c=1, at τ=1 two ways: exactly by numerical methods and by the approximate "high - τ" expression (26). The discrepancy was 3%, an amount nearly invisible on the scale of Fig. 1. The results should therefore be adequately reliable for all $\tau > 1$.

The temperature-dependence is seen to be quite different in the two cases (note that the log-log scales tend to mask the differences). Basically, we find a T^6 dependence for restrahl coupling, T^4 and U-center coupling.

Thus, experiments with crystals containing different concentrations of impurities should provide a different temperature dependence of the absorption as well as a different magnitude of the absorption at any given temperature - provided impurities are at all active in initiating absorption. For large impurity concentrations, one would expect a T^4 dependence. As the impurity concentration goes down, one would expect not only a decrease in the absolute value of the absorption, but also a shift in the temperature dependence to T^6. If the latter effect does not occur as one approaches the purest crystal one can find, one would conclude that enough impurities remain to dominate the absorption process, and that further purification might result in even smaller absorption; if it does occur one would conclude that the absorption is "intrinsic" and not capable of being further reduced.

5.4. Summary

We have attempted to calculate the temperature dependence of absorption of light by an ionic crystal in the far infrared, on basis of the following assumptions.

1. Absorption is caused by lattice vibrations (phonons), and the energy of the light absorbed is so large as to require many phonons.

2. Temperature dependence enters the problem via phonon population factors only (i.e. via a Bose distribution for phonons, or, equivalently, a Boltzman distribution for oscillator states)

3. The frequency spectrum of the crystal can be approximated by a Debye distribution.

4. Higher-order processes are much more improbable than lower-order ones.

5. Energy conservation for the conversion of one photon into n phonons is taken into account, but momentum conservation is ignored.

As a consequence of assumption 4, only summation processes, not difference processes, have been considered; also, 2. and 4. together implied that the mechanism for the multiphonon absorption (e.g. anharmonicity or high-order electric moments) did not have to be specified. Assumption 3, though well-known to be very far from quantitatively accurate, is probably quite mild in its effect compared to 5, particularly since the distribution is in each case the distribution is integrated over.

With these assumptions, we found that measurement of the temperature dependence of the absorption should enable one to ascertain whether absorption is caused by intrinsic lattice properties or by the effects of light impurities.

Appendix I

Our purpose here is to define certain discontinuous functions and give some complex representations for them that are useful in Section II.

For any integer $n > 0$ let us define

$$S_n(t) = \begin{cases} t^n/n! & t > 0 \\ 0 & t < 0 \end{cases} . \qquad \text{(A1)}$$

$S_0(t)$ is the well known "Heaviside" or step function that is 0 or 1 according as $t \lessgtr 0$. S_0 has the representation

$$S_0(t) = (2\pi i)^{-1} \int_{\gamma - i\omega}^{\gamma + i\omega} (ds/s)\, e^{ts} , \qquad \text{(A2)}$$

γ being any real, positive number. n - fold integration of (A2) from $-\infty$ to t gives

$$S_n(t) = (2\pi i)^{-1} \int_{\gamma - i\omega}^{\gamma + i\omega} (ds/s)\, e^{ts} s^{-n} \qquad \text{(A3)}$$

and differentiation of (A2) gives the delta function

$$\delta(t) = (2\pi i)^{-1} \int_{\gamma - i\omega}^{\gamma + i\omega} ds\, e^{ts} . \qquad \text{(A4)}$$

Appendix II

Derivation of Equation (5) and (6)

A brief derivation of Eqs. (5) and (6) may be of interest here, even though the formulas are not new. Our object is to exhibit the paucity of assumptions needed and hence the generality.

It can be shown that any system involving weakly interacting bosons leads to an emission probability for boson a proportional to $n_a + 1$ and to an absorption probability for the same proportional to n_a itself; here n_a is the number of bosons originally in state a. (Ref. 1, section 61, Eqs. (40), (47) (50), (51).) Simultaneous emission of k bosons in states $a_1, a_2, \ldots a_k$ respectively is then proportional to $(1+n_{a_1})(1+n_{a_2})\ldots(1+n_{a_k})$ and absorption similarly to $n_{a_1} n_{a_2} \ldots n_{a_k}$. If the bosons involved are phonons in a solid and absorption (emission) of phonons of energy $E_a, E_b, \ldots, E_k$ is accompanied by emission (absorption) of one photon of energy then the net absorption probability of a photon of such energy is given by

$$\prod_{i=1}^{k} (1+n_i) - \prod_{i=1}^{k} n_i$$

Summations over the individual states a, b, c... available, respectively, to boson, 1, 2, 3 according to Bose-Einstein statistics then leads to Eqs. (5), (6).

References

1. P. A. M. Dirac, Principles of Quantum Mechanics, 3rd edition, (Oxford, 1947).

2. J. E. Mayer and M. G. Mayer, Statistical Mechanics (Wiley, New York, 1947) p. 370.

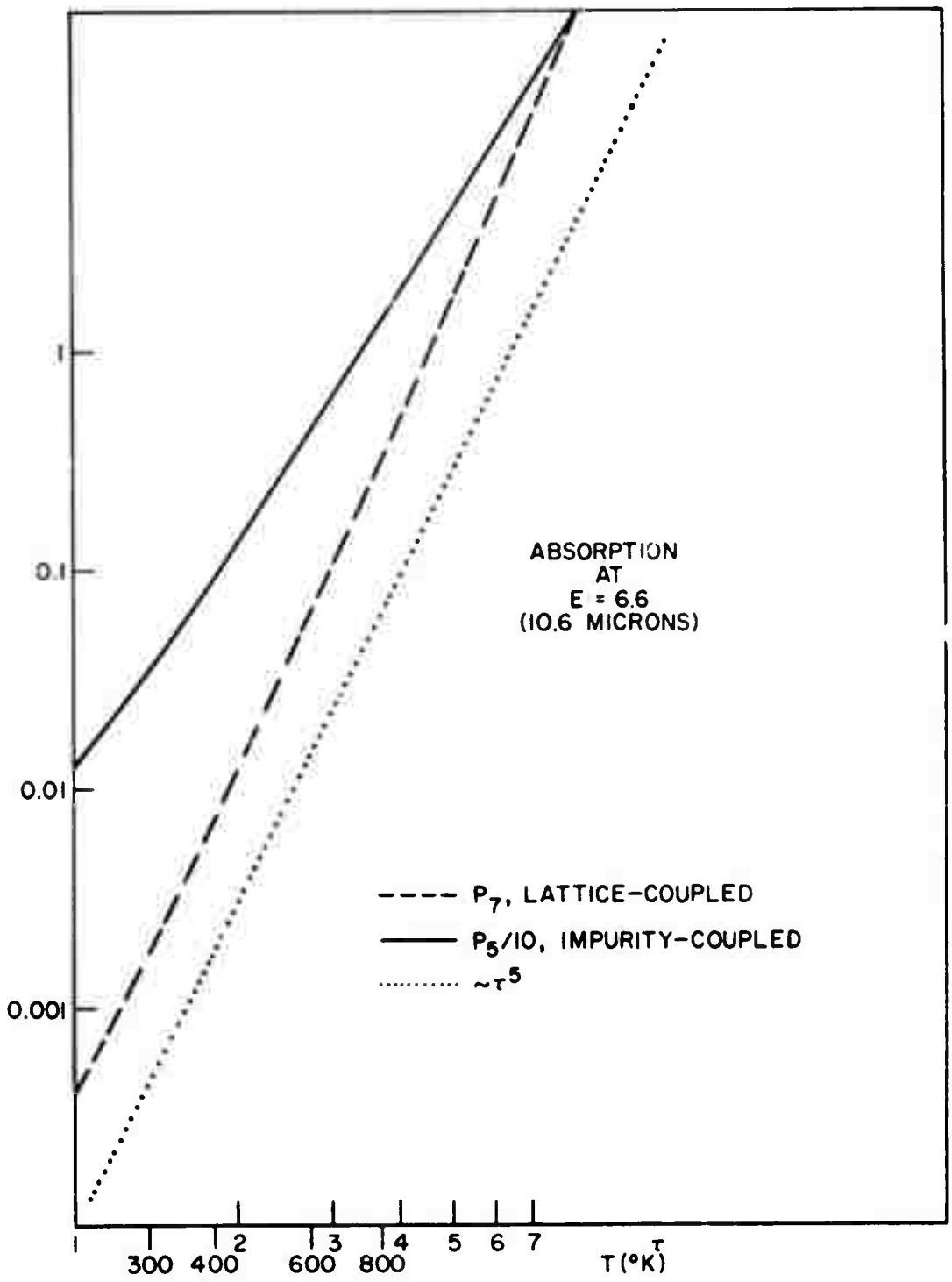

Fig. 1. Temperature Dependence of Absorption of KCl at 10.6 microns. A. From a 5-phonon process with coupling of a phonon to a U-center (solid curve). B. From a 7-phonon process with coupling of phonon to Restrahl oscillator (dashed curve). The dotted curve gives T-dependence for comparison.